United Aircraft Research Laboratories

U
UNITED AIRCRAFT CORPORATION
A

EAST HARTFORD, CONNECTICUT

D-910092-4

Theoretical Investigation of the
Opacity of Heavy-Atom Gases

NASA Contract No. NASw-847

REPORTED BY *N. L. Krascella*

N. L. Krascella

APPROVED BY

F. S. Owen
Chief, Propulsion

DATE September 1965

NO. OF PAGES 52   COPY NO. 17

FOREWORD

An exploratory experimental and theoretical investigation of gaseous nuclear rocket technology is being conducted by the United Aircraft Corporation Research Laboratories under Contract NASw-847 with the joint AEC-NASA Space Nuclear Propulsion Office. The Technical Supervisor of the Contract for NASA is Captain W. A. Yingling (USAF). Results of the investigation conducted during the period between September 15, 1964 and September 15, 1965 are described in the following eleven reports (including the present report) which comprise the required third Interim Summary Technical Report under the Contract:

1. McFarlin, D. J.: Experimental Investigation of the Effect of Peripheral Wall Injection Technique on Turbulence in an Air Vortex Tube. UAC Research Laboratories Report D-910091-5, September 1965. (Unclassified)

2. Johnson, B. V.: Analytical Study of Propellant Flow Requirements for Reducing Heat Transfer to the End Walls of Vortex-Stabilized Gaseous Nuclear Rocket Engines (U). UAC Research Laboratories Report D-910091-6, September 1965. (report classified Confidential)

3. Travers, A.: Experimental Investigation of Peripheral Wall Injection Techniques in a Water Vortex Tube. UAC Research Laboratories Report D-910091-7, September 1965. (Unclassified)

4. Johnson, B. V., and A. Travers: Analytical and Experimental Investigation of Flow Control in a Vortex Tube by End-Wall Suction and Injection (U). UAC Research Laboratories Report D-910091-8, September 1965. (report classified Confidential)

5. Mensing, A. E., and J. S. Kendall: Experimental Investigation of the Effect of Heavy-to-Light-Gas Density Ratio on Two-Component Vortex Tube Containment Characteristics (U). UAC Research Laboratories Report D-910091-9, September 1965. (report classified Confidential)

6. Krascella, N. L.: Theoretical Investigation of the Opacity of Heavy-Atom Gases. UAC Research Laboratories Report D-910092-4, September 1965. (Unclassified) (present report)

7. Kesten, A. S., and R. B. Kinney: Theoretical Effect of Changes in Constituent Opacities on Radiant Heat Transfer in a Vortex-Stabilized Gaseous Nuclear Rocket (U). UAC Research Laboratories Report D-910092-5, September 1965. (report classified Confidential)

8. Marteney, P. J., N. L. Krascella, and W. G. Burwell: Experimental Refractive Indices and Theoretical Small-Particle Spectral Properties of Selected Metals. UAC Research Laboratories Report D-910092-6, September 1965. (Unclassified)

9. Williamson, H. A., H. H. Michels, and S. B. Schneiderman: Theoretical Investigation of the Lowest Five Ionization Potentials of Uranium. UAC Research Laboratories Report D-910099-2, September 1965. (Unclassified)

10. McLafferty, G. H., H. H. Michels, T. S. Latham, and R. Roback: Analytical Study of Hydrogen Turbopump Cycles for Advanced Nuclear Rockets. UAC Research Laboratories Report D-910093-19, September 1965. (Unclassified)

11. McLafferty, G. H.: Analytical Study of the Performance Characteristics of Vortex-Stabilized Gaseous Nuclear Rocket Engines (U). UAC Research Laboratories Report D-910093-20, September 1965. (report classified Confidential)

Report D-910092-4

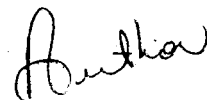Theoretical Investigation of the Opacity of Heavy-Atom Gases

TABLE OF CONTENTS

Theoretical Investigation

of the Opacity of Heavy-Atom Gases

SUMMARY

\|A579

    A theoretical investigation was conducted to determine the composition,
spectral absorption coefficients and Rosseland mean opacity of gaseous nuclear
fuel and tungsten using a semi-empirical heavy-atom analytical model in order
to obtain information applicable to gaseous nuclear rockets. The characteristics
of the nuclear fuel were determined for a range of values of each of the
following parameters which must be assumed in using the heavy-atom model;
ionization potentials, energy level spacings, total oscillator strengths, and the
ratio of partition functions for successive ionization species. Included in
these ranges of values were calculated ionization potentials and partition
function ratios. The greatest changes in Rosseland mean opacity at a given
pressure and temperature resulted from the calculated changes in fuel ioniza-
tion potentials. The Rosseland mean opacity of gaseous tungsten was calculated
on the basis of completely overlapped lines (which would result from line
broadening due to the presence of a perturbing gas at infinite pressure), and for
finite-width spectral lines due to the presence of specified values of hydrogen
partial pressure.

CONCLUSIONS

1. A change in the ionization potentials of gaseous nuclear fuel from values of 6, 10, 18, and 28 ev (which were assumed in the preceding studies) to values of 6, 17, 39 and 66 ev (which represent the latest theoretical estimates) results in substantial changes in the composition, spectral absorption coefficients and Rosseland mean opacity of the nuclear fuel.

2. Substantial changes in the ratio of partition functions for successive ionization species generally have a small effect on the composition, spectral absorption coefficients and Rosseland mean opacity of the nuclear fuel.

3. Substantial changes in the energy level spacings and total oscillator strengths (which have no effect on the composition, according to the heavy-atom model) result in a very small change in the Rosseland mean opacity of the nuclear fuel.

4. The presence of hydrogen at high pressures causes sufficient broadening of the spectral lines in low-pressure tungsten gas to fill in a major portion of the windows between the spectral lines. The resulting Rosseland mean opacities of tungsten gas for a hydrogen pressure of 1000 atm are on the order of half of those with completely overlapped lines.

5. The greatest uncertainties in the spectral absorption coefficients calculated from the heavy-atom model occur at low wave numbers (long wavelengths). These uncertainties would have little effect on the Rosseland mean opacities of gaseous nuclear fuel at high temperatures, but may have a substantial effect on the Rosseland mean opacities of gaseous tungsten at low temperatures.

INTRODUCTION

Analytical studies of the feasibility and performance capability of gaseous nuclear rocket engines, such as that described in Ref. 1, require knowledge of the composition, spectral absorption coefficients and mean opacity of the fuel, seed and propellant species involved in order to determine the temperature and heat flux distributions within the engine. The extreme complexity of the spectra and lack of requisite atomic data (e.g., ionization potentials, energy levels...) for the heavy-atom nuclear fuel and seed preclude an exact theoretical determination of the composition and optical properties of these gases. Thus, in previous radiant heat transfer analyses of gaseous nuclear rocket engines conducted at UARL, a semiempirical heavy-atom model (Refs. 2, 3, and 4) was developed to estimate the prerequisite gas properties of the nuclear fuel. These estimated heavy-atom gas properties are subject to uncertainties in the ionization potentials, energy level spacings, total oscillator strengths and a partition function parameter used as input model parameters. In addition, these predicted gas properties may be incorrect at low temperatures where vaporized heavy-atom seeds might be used to augment hydrogen propellant opacity because the theoretical model was intended for use at temperatures above approximately 10,000 K (18,000 R) in the nuclear fuel region. Above a temperature of about 10,000 K the continuum approximation used to calculate the bound-bound spectral absorption coefficients was justified on the basis of strong electron broadening of discrete lines (Ref. 4). On the other hand below approximately 10,000 K, collision broadening by neutral molecular and atomic hydrogen predominates but is insufficient to cause strong line overlapping. Therefore, the continuum approximation in the line region is no longer valid in the seed-propellant region.

Based on the preceding discussion, it is apparent that two areas of investigation of the theoretical heavy-atom model are indicated. Thus, the objectives of the work described herein are: To determine the sensitivity of composition, spectral absorption coefficients and Rosseland mean opacities to changes in the model parameters and to calculate the spectral absorption coefficients and Rosseland mean opacity of vaporized tungsten using the basic heavy-atom model described in Ref. 4 but modified to account for insufficient line overlapping in the bound-bound spectral region.

ANALYTICAL HEAVY-ATOM MODEL

The composition, spectral absorption coefficients and Rosseland mean opacities of heavy-atom gases previously employed in radiant heat transfer analyses of gaseous nuclear rocket engines at UARL were based on a semiempirical heavy-atom model described in Refs. 2, 3 and 4. A brief description of the model is given in the following paragraphs.

In the model, each ionization species considered (e.g., the neutral atom, singly ionized atom) consists of a number of equally spaced energy levels or term values designated by $(E_n)_i$, between the ground state, $(E_O)_i$, and the ionization potential of the ith ionization species, I_i. A typical energy level scheme is shown in Fig. 1. Transitions are allowed between all energy levels subject to a specified oscillator strength distribution. (The oscillator strength or f-number associated with a transition is proportional to the probability that the transition will occur.) A representative transition between energy level n and n' is depicted by the quantity $(\Delta E_{n,n'})_i$ in Fig. 1. Because detailed information about oscillator strengths for bound-bound transitions in heavy-atom elements is, at best, meager, the oscillator strength dependence on photon energy described below was used for each ionization species.

A hydrogenic distribution of oscillator strength per unit photon energy, df/dE, was assumed to apply in the bound-free spectral region as illustrated in Fig. 2, that is

$$df/dE \sim 1/E^3 \tag{1}$$

It was assumed that df/dE could be extrapolated into the bound-bound spectral region according to Eq. (1) up to a cut-off energy, $(E^o)_i$ (see Fig. 2). From E = 0 to E = $(E^o)_i$, df/dE was made constant. The cut-off in the extrapolation at $(E^o)_i$ was necessary to limit the total area under the curve shown in Fig. 2 to a value equal to the total oscillator strength as required by the oscillator strength sum rule (Ref. 5).

The machine program for calculating heavy-atom gas properties as described in Ref. 4 requires three parameters as input for each of the four fuel ionization species $(F^o, F^+, F^{++}, F^{+++})$ involved. These parameters are: the ionization potentials, energy level spacings and total oscillator strengths. In addition it is necessary to specify a single value for the partition function parameter as required by the Saha equations (Ref.5) which describe the composition in terms of possible ionization species derived by repetitive ionization of the parent

heavy-atom gas. The Saha equations are given by:

$$\frac{N_{i+1}}{N_i} \; N_e \; = \; KT^{3/2} G \; \exp\left\{ -I_i / kT \right\} \tag{2}$$

The quantity G in Eq. (2) is the ratio of the partition function for ionization species $i+1$ to the partition function for ionization species i :

$$G \; \equiv \; Q_{i+1} / Q_i \tag{3}$$

The parameter G , as employed in the machine program, is a constant independent of i at a given temperature.

FUEL CHARACTERISTICS DETERMINED FROM PARAMETRIC STUDY OF HEAVY-ATOM MODEL

The composition, spectral absorption coefficients and Rosseland mean opacity of nuclear fuel determined by the heavy-atom model of Ref. 4 are a function of the absolute values of several input parameters used to define the model. To determine the effect of changes in these input parameters on the calculated fuel characteristics, a series of cases were evaluated in which the values of these input parameters were systematically altered. Twelve cases were calculated; values of the input parameters employed in each case are given in Table I. Case 1 is used as a reference case; values of parameters for this case are identical to those employed in Ref. 4.

Composition

Four fuel ionization species, F°, F^+, F^{++}, and F^{+++} are treated in the composition subroutine of the heavy-atom model machine program. The densities of these species at any temperature and pressure are determined by inputting ionization potentials for F°, F^+ and F^{++} and a single value of the partition function parameter. The composition in terms of ionization species is independent of the total oscillator strengths and the energy level spacings. Therefore, the effect of changes in the values of the model parameters on composition was determined only for changes in the partition function ratios and ionization potentials.

Effect of Changes in Partition Function Parameter

As defined in the composition subroutine, the partition function parameter G, is a constant and identical for all partition function ratios

$$G = Q_{F^+}/Q_{F^\circ} = Q_{F^{++}}/Q_{F^+} = Q_{F^{+++}}/Q_{F^{++}} \tag{4}$$

where Q_{F^+}/Q_{F°, $Q_{F^{++}}/Q_{F^+}$ and $Q_{F^{+++}}/Q_{F^{++}}$ are the partition function ratios. In addition, G is usually assumed to be independent of temperature. However, a temperature-dependent partition function parameter was determined for use in one set of calculations by directly computing the partition functions Q_{F°, Q_{F^+}, $Q_{F^{++}}$ and $Q_{F^{+++}}$ for each ionization species based on the energy level distribution required by the model:

$$Q_i \sim \sum_n \exp\left\{-(E_n)_i / kT\right\} \tag{5}$$

where

$$(E_n)_i = n a_i \; ; \; n = 0,1,2,3 \ldots (I_i / a_i) - 1 \tag{6}$$

The four partition functions calculated by direct summation according to Eq. (5) are plotted in Fig. 3 as a function of temperature. Similarly, the partition function ratios calculated from the results of Fig. 3 are plotted in Fig. 4 as a function of temperature. Because the machine program requires only a single value for the parameter G, the ratios given in Fig. 4 were averaged at each temperature of interest as follows:

$$G = \frac{1}{3} \left\{ \frac{Q_{F^+}}{Q_{F^0}} + \frac{Q_{F^{++}}}{Q_{F^+}} + \frac{Q_{F^{+++}}}{Q_{F^{++}}} \right\} \tag{7}$$

The results of this averaging are shown in Fig. 5 as a function of temperature and were used to compute the fuel composition. Also plotted in Fig. 5 are the temperature independent partition function parameters employed in Case 1, the reference case, and Case 7. Case 7 represents an arbitrary change in the partition function parameter by a factor of 5.

The values of the partition function parameter described for Cases 1, 7 and 10 were used with a consistent set of ionization potentials, energy level spacings and total oscillator strengths for all three cases (see Table I) to compute the composition, spectral absorption coefficients and Rosseland mean opacity for a total pressure of 1000 atm. The composition results are illustrated in Fig. 6. The differences in composition resulting from the parametric values used for Case 10 as compared to Case 1 are not significant. For example, at 40,000 K the density of F^+ is of the order 1.3×10^{18} cm^{-3} for Case 1 ($G = 1$) compared with a value of 1.0×10^{18} cm^{-3} for Case 10 ($G = 1.07$). For higher temperatures the differences in composition between Cases 1 and 10 are greater since the differences in values of G in Case 1 and 10 are greater. Conversely, the relatively large ratio between G's for Cases 1 and 7 ($G_7 / G_1 = 5.0$) was expected to give correspondingly large differences in composition as confirmed by the results shown in Fig. 6.

Effect of Changes in the Ionization Potentials

As stated previously, the composition also depends upon the values selected for the ionization potentials of species F^0, F^+ and F^{++}. Three cases identical with respect to all parameters except the ionization potentials (see Table I) were used to ascertain the effect of change in ionization potentials upon the gas composition.

These are Cases 1, 11 and 12. Case 11 differed from Case 1 (the reference case) in that the ionization potentials for successive ionization species were arbitrarily made equal to twice the value of the preceding ionization species. The ionization potentials used in Case 12, on the other hand, represent current estimates of the first four ionization potentials for the nuclear fuel (uranium) as described in Ref. 6. Comparisons of the composition results for Cases 1 and 12 are made in Figs. 7 to 9 for total pressures of 100, 500 and 1000 atm respectively. The results for Case 11 are not shown on these figures but would lie between the curves for Cases 1 and 12 at any given temperature. The increase in magnitude of the ionization potentials for F°, F^{+} and F^{++} results in marked changes in the composition at any temperature as is shown in Figs. 7 to 9. The higher ionization potentials employed in Case 12 delay the appearance of a specific ionization species at any given temperature. Comparing Fig. 6 with Figs. 7 to 9, it is evident that changes in the ionization potentials exert more pronounced influence on the fuel composition than do changes in the partition function parameter.

Summary of Effects of Changes in Parameters on Composition

The composition was appreciably altered by changes in the ionization potentials and to a lesser degree by changes in the partition functions parameter. The effect of introducing a temperature dependent partition function parameter on composition was negligible.

Because the energy level spacings and total oscillator strengths do not enter the equations for composition, no changes in composition were evident for Cases 2 to 6 and 8 and 9. The composition results for these Cases (2 to 6, 8 and 9) are identical with Case 1.

Spectral Absorption Coefficients

The spectral absorption coefficients of the nuclear fuel estimated by means of the heavy-atom model are based on specification of the complete set of model parameters. The spectral absorption coefficients were calculated for all 12 cases listed in Table I at temperatures of 20,000 K, 60,000 K and 100,000 K for a total pressure of 1000 atm. The results of these calculations for the 12 cases are compared in Fig. 10 for 20,000 K, Fig. 11 for 60,000 K and Fig. 12 for 100,000 K. (Reference should be made to Table I for the parametric variations associated with each case.)

Effect of Changes in Energy Level Spacings

Cases 1 to 3 involve changes in the energy level spacing a_i, from 0.4 to 0.05 ev. Ionization potentials, total oscillator strengths and the partition function parameter are the same in Cases 1 to 3. As shown in Figs. 10 to 12, no significant differences occur in the spectral absorption coefficients as a result of

these changes in the energy level spacing parameter. (Slight increases in the spectral absorption coefficients occur at wave numbers below approximately 10,000 cm^{-1}.)

Effect of Changes in Total Oscillator Strengths

Cases 4 to 6 differ from Cases 1 to 3 in that the total oscillator strengths were reduced from a value of 2 to a value of 1, while the energy level spacings were decreased as in Cases 1 to 3 from 0.4 to 0.05 ev. Since the area under a plot of absorption coefficient against wave number is proportional to the total oscillator strength, the spectral absorption coefficients for Cases 4 to 6 were expected to lie somewhat below those for the reference case. The results shown in Figs. 10 to 12 exhibit this behavior. The slight increase in the spectral absorption coefficients with a decrease in level spacing at wave numbers below approximately 10,000 cm^{-1} noted in Cases 1 to 3 is also evident in Cases 4 to 6.

Effect of Changes in Partition Function Parameter

Case 7 differed from Case 1 in that the partition function parameter G , was increased by a factor of 5. (The effect of this parametric change on composition was illustrated in Fig. 6.) Although the spectral absorption coefficient is not directly related to the partition function parameter, the effect of a change in this parameter on absorption coefficients is reflected through the altered composition. At 20,000 K (see Fig. 10), the spectral absorption coefficient is seen to be reduced by a factor of approximately 1.8 in a wave number interval between 1000 cm^{-1} and approximately 15,000 cm^{-1}. Because the total oscillator strengths assumed for Cases 1 and 7 are identical, the spectral absorption coefficients for Case 7 must exceed those for Case 1 over part of the spectral range. The curves for Cases 1 and 7 do intersect at a wave number of approximately 36,000 cm^{-1} as shown in Fig. 10. Beyond 36,000 cm^{-1} the spectral absorption coefficients for Case 7 exceed those for Case 1 as required by the oscillator strength sum rule (ref. 5). At 60,000 K (Fig. 11) and 100,000 K (Fig. 12), the absorption coefficients for Case 7 and Case 1 are effectively identical. This agreement is due to the fact that, above temperatures of approximately 60,000 K, F^{+++} is the dominant ionization species contributing to the absorption coefficient (see Fig. 6). Above approximately 60,000 K the particle densities for F^{+++} in Cases 1 and 7 are the same.

Effect of Multiple Changes in Energy Level Spacings and Total Oscillator Strengths

In Case 8, each ionization species was assigned a different value for the energy level spacing while in Case 9 each ionization species was assigned a different value for the total oscillator strength. All other parameters were identical to those used in Case 1 (see Table I). The spectral absorption coefficient results are shown in Figs. 10 to 12 for temperatures of 20,000, 60,000, and 100,000 K at a total pressure of 1000 atm. At a temperature of 20,000 K and for wave numbers less than approximately 20,000 cm^{-1}, the ratio of the spectral absorption coefficient

for Case 8 to the spectral absorption coefficient for Case 9 is about 3.7 (see Fig. 10). As seen in Fig. 6, the principal species contributing to the spectral absorption coefficient at a temperature of 20,000 K are F° and F^{+}. (The composition for Cases 1, 8, and 9 are identical.) Therefore, the marked decrease in the absorption coefficient in Case 9 is attributed to the reduced values used for the total oscillator strengths for F° and F^{+} (see Table I). At temperatures of 60,000 K and 100,000 K (Figs. 11 and 12, respectively) the spectral absorption coefficients for Cases 8 and 9 are essentially equivalent at all wave numbers. For these temperatures, the dominant species contributing to the absorption coefficient is F^{+++} as shown in Fig. 6. The total oscillator strength for species F^{+++} is the same in Cases 8 and 9, thus no appreciable difference in spectral absorption coefficient is evident.

Effect of Changes in Ionization Potentials

Cases 11 and 12 are similar and involve changes in the assigned ionization potentials for ionization species F°, F^{+}, F^{++}, and F^{+++}. Case 11 was a preliminary attempt to assess the effect of changes in ionization potentials on the composition and spectral properties prior to receipt of the theoretical estimates of these quantities which are presented in Ref. 6. The spectral data (absorption coefficient vs. wave number) for Case 12, based on the current estimate for the ionization potentials given in Ref. 6, are plotted for three temperatures (10,000, 50,000, and 100,000 K) for a total pressure of 100 atm in Fig. 13, 500 atm in Fig. 14, and 1000 atm in Fig. 15. Corresponding data for Case 1 (reference case) are shown for comparison. The differences in spectral absorption coefficients between Cases 1 and 12 (between Cases 1 and 11 also) are attributable to the change in the fuel composition and oscillation strength distribution with wave number which results from the higher ionization potentials employed in Case 12. For example, at a temperature of 10,000 K and at a pressure of 1000 atm (see Fig. 15), the particle densities of F° and F^{+} are approximately equal for Cases 1 and 12 (see Fig. 9). Because the potentials employed in Case 12 considerably exceed those used in Case 1 (see Table I), the effective oscillator strength per unit wave number is reduced for Case 12, thereby causing the decrease in spectral absorption coefficients in the bound-bound region over those for Case 1. Since the area under the curve must be identical for both cases (the same oscillator strength was used for Cases 1 and 12), the spectral absorption coefficient for Case 12 becomes greater than that for Case 1 above a wave number of approximately 30,000 cm^{-1}. Similar results are observed for temperatures of 50,000 and 100,000 K; the same reasoning applies.

Summary of Effects of Changes in Parameters on Spectral Absorption Coefficients

In summary, the following observations are made with respect to the effect of changes in model parameters on the spectral absorption coefficients;

1. At high temperatures and for wave numbers less than approximately 100,000 cm^{-1} the only significant effects on spectral absorption coefficients result from changes in the total oscillator strengths and ionization potentials.

2. At high temperatures and for wave numbers greater than approximately 100,000 cm^{-1} the only significant changes in spectral absorption coefficients occur as a result of changes in the ionization potentials.

3. At low temperatures, only limited effects are observed in the spectral absorption coefficients at wave numbers greater than approximately 100,000 cm^{-1} for all parametric changes except for changes in the ionization potentials or the partition function parameter. At wave numbers less than approximately 100,000 cm^{-1}, changes in the ionization potentials, level spacings and, to a limited extent, partition functions have a limited effect on the spectral absorption coefficients.

Rosseland Mean Opacity

Effect of Changes in Model Parameters

The Rosseland mean opacity is defined by the following equations (Refs. 2 and 3):

$$a_R = \frac{\int_o^\infty \frac{\partial B_\omega}{\partial T} \, d\omega}{\int_o^\infty \frac{1}{a_\omega^*} \frac{\partial B_\omega}{\partial T} \, d\omega} \tag{8}$$

where

$$B_\omega = \frac{2hc^2\omega^3}{e^{hc\omega/kT} - 1} \tag{9}$$

and

$$\frac{\partial B_\omega}{\partial T} = \frac{2h^2c^3\omega^4}{kT^2} \frac{e^{hc\omega/kT}}{(e^{hc\omega/kT} - 1)^2} \tag{10}$$

For each case (1 through 12), the Rosseland mean opacity was calculated for several temperatures between 10,000 K and 100,000 K. These calculated results are summarized in Table II as the ratio of Rosseland mean opacity for any particular case to that for the reference case, Case 1: $a_R/(a_R)_{CASE\ 1}$. For Case 1, however, the actual magnitudes calculated for the Rosseland mean opacity are listed.

As shown in Table II, no significant differences in Rosseland mean opacity are observed (ratios near 1.0) for Cases 2 through 6 and 8 through 10. For Cases 7, 11 and 12 appreciable changes in the Rosseland mean opacity are noted. The results for these cases, $a_R/(a_R)_{CASE\ 1}$ vs. T are illustrated in Fig. 16. At a temperature of 20,000 K, approximately 86 percent of black-body energy is at wave numbers above 25,000 cm^{-1}; therefore, parametric variations which change the spectral absorption coefficients above a wave number of about 25,000 cm^{-1} should exert the greatest influence on Rosseland mean opacity. The spectral absorption coefficients are plotted in Fig. 10 for a temperature of 20,000 K. The slight increase in spectral data for Case 7 above the 25,000 cm^{-1} limit compared with that for Case 1 gives rise to the slightly greater Rosseland mean opacity: $a_R/(a_R)_{CASE\ 1} \simeq 1.43$. The same argument applies to Cases 11 and 12.

At 60,000 K, approximately 74 percent of the black-body energy is in the spectral region above a wave number of about 100,000 cm^{-1}. As shown in Fig. 11, only Cases 11 and 12 have spectral absorption coefficients greater than those for Case 1 above the 100,000 cm^{-1} limit. As a result, the Rosseland mean opacity ratio, shown in Fig. 16, is appreciably greater than unity for Cases 11 and 12 but not for Case 7. Similar results apply for higher temperatures.

Rosseland mean opacity is plotted as a function of temperature in Fig. 17 for Cases 1 and 12 at three total pressures: 100, 500 and 1000 atm. At a temperature of 100,000 K, the Rosseland mean opacity for Case 12 is greater than that for Case 1 by a factor of about 7.1 for all pressures. This ratio of Rosseland mean opacities decreases as the temperature is decreased, the factor being of the order of 1.3 at a temperature of 20,000 K. Case 12 currently represents the best available estimate of fuel opacity.

Effect of Spectral "Windows"

As a supplement to the study of the effect of changes in model parameters on the composition, spectral absorption coefficients and Rosseland mean opacity of nuclear fuel, based on the heavy-atom model, a preliminary analysis was made to ascertain the effect on Rosseland mean opacity of different distributions of absorption coefficient with wave number in the bound-bound spectral region. In Fig. 18, the three absorption coefficient distributions used in the analysis are illustrated (absorption coefficient without stimulated emission vs. wave number). The total oscillator strength (proportional to the total area under the curve) was the same for each distribution. In addition, the partial oscillator strengths assigned to

the bound-free region ($\omega \geq 50,000$ cm^{-1}) and the bound-bound region ($\omega < 50,000$ cm^{-1}) were identical for each distribution. Distribution A is analagous to that generated by the heavy-atom model for a specified ionization species at any arbitrary temperature (see Fig. 2). Distributions B and C represent inclusion of spectral "windows" in the bound-bound region.

The Rosseland mean opacity was computed for each spectral absorption coefficient distribution in Fig. 18 based on the assumption that these distributions were constant with temperature. However, inclusion of stimulated emission factors in the spectral absorption coefficient prior to computations of the Rosseland mean opacity does impart a degree of temperature dependence. The Rosseland mean opacities corresponding to the three spectral distributions of Fig. 18 are plotted in Fig. 19 as a function of temperature. Except for a small difference in the Rosseland mean opacity at 10,000 K which decreases as the temperature is increased, no appreciable change occurred in the Rosseland mean opacity as a result of including spectral "windows" in the bound-bound region. If these "windows" were placed in the spectrum at higher wave numbers (to simulate "windows" in a highly ionized species), the general characteristic differences shown in Rosseland mean opacity for 10,000 K would also be present at higher temperatures. However, the differences shown for a temperature of 10,000 K are small.

OPTICAL PROPERTIES OF GASEOUS TUNGSTEN SEEDS

The propellant in a gaseous core nuclear rocket must be sufficiently opaque to absorb almost all of the thermal radiation approaching the reaction chamber walls from the nuclear fuel region. At high pressures and at temperatures below approximately 8000 K (14,400 R), the hydrogen propellant is essentially transparent to thermal radiation; hence, an opaque seeding agent is required to augment the propellant opacity. Thus additional opacity might be provided by a material such as tungsten. Tungsten would provide opacity below its boiling point (about 5645 K) as small condensed particulate matter and above its boiling point as a vapor having line and continuum spectral absorption. The spectral absorption coefficients of small solid tungsten particles were estimated and reported in Refs. 7, 8, 9, and 10. Preliminary estimates of the spectral absorption coefficients of tungsten vapor, based on the heavy-atom model described in Ref. 4, are presented and discussed in the following section of this report.

Effect of Non-Overlapping Lines on Mean Opacity

As was indicated in a previous section of this report, the heavy-atom model described in Ref. 4 utilizes a continuum approximation for the bound-bound spectral absorption coefficients. At temperatures above approximately 10,000 K, the continuum approximation was justified on the basis of strong electron broadening of the individual spectral lines as was discussed in Ref. 4. As a result of the electron broadening predicted, adjacent spectral lines in the model were strongly overlapped. Thus, individual line contours were of no relevance in the bound-bound spectral absorption coefficient calculations. The discrete structure, exhibiting marked wave number dependence normally associated with the line region of the spectrum, was replaced by a continuum which varied slowly with wave number.

In the temperature region applicable to gaseous seed-propellant mixtures (below approximately 8,000 K), collision broadening by atomic and molecular hydrogen predominates rather than electron broadening. Resonance (self) broadening in the seed material is negligible since the density of seed material is small compared to the density of the hydrogen propellant. Maximum estimated half-widths based on collision broadening are of the order of 6 cm^{-1} as compared to separation between lines of the order of 50 cm^{-1} (see following section), thus strong line overlapping does not occur. As a result, discrete line structure should be evident and the continuum approximation used in the heavy-atom model no longer applies.

The heavy-atom model (assuming completely overlapped lines) may be used to estimate an upper limit for the Rosseland mean opacity of gaseous tungsten seed. To correct this Rosseland mean opacity for non-overlapping line effects, the following treatment and correction factors were devised. The effect of the ratio of line

half-width to line spacing, Γ/S, for equally-spaced, equal strength, adjacent lines on the ratio of the average local mean opacity to the average local mean opacity defined in terms of the mean free path was computed (see equations - Fig. 20). This ratio, $\bar{\bar{a}}/\bar{a}$, is approximately equivalent to the ratio of the Rosseland mean opacity with discrete lines to the Rosseland mean opacity based on a continuum approximation ($\Gamma/S \gg 1$) for the line region of the spectrum. A plot of $\bar{\bar{a}}/\bar{a}$ is presented in Fig. 20. Also presented in Fig. 20, is the ratio of the minimum value of the spectral absorption coefficient between two adjacent lines to the corresponding maximum value of the absorption coefficient occurring at a line center.

The results of Fig. 20 show that for Γ/S equal to 0.45, the ratio of the minimum to maximum absorption coefficient is approximately 0.75. The value of $\bar{\bar{a}}/\bar{a}$ at $\Gamma/S = 0.45$ is approximately 1.0. Therefore above a Γ/S of approximately 0.45, the slight line structure evident (indicated by $(a_\omega)_{MIN}/(a_\omega)_{MAX} \simeq 0.75$) does not affect the Rosseland mean opacity (that is $\bar{\bar{a}}/\bar{a} \simeq 1$). As Γ/S decreases, indicating a more pronounced line structure, the Rosseland mean opacity with line structure included becomes much less than that calculated assuming completely overlapped lines.

Average Line Spacing in Heavy-Atom Elements

As a prerequisite to the determination of the discrete line effect in the bound-bound region of gaseous tungsten, a review of the current literature was made to determine average line spacing in heavy-atom elements. Four elements were investigated; hafnium, molybdenum, niobium, and tungsten. Lines of known intensity and wave number associated with each of the elements listed above are tabulated in Ref. 11. The number of lines appearing in each wave number interval of 1000 cm^{-1} were determined and an average line spacing in each 1000 cm^{-1} interval was computed. These results are plotted in Fig. 21. Also indicated on the right of the graph by horizontal lines are the overall average value of the line spacing in the total wave number interval in which the known lines are observed (e.g., for tungsten, $S \simeq 32$). From Ref. 12, data for the total number of lines in each species in a given wave number interval independent of intensity assignments are reported. The average line spacing in the total wave number interval based on these data are indicated by horizontal lines to the left of the curves in Fig. 21 (e.g., for tungsten, $S \simeq 13$). Since more lines are reported in the latter case, the overall average line spacings based on these data are somewhat less than those calculated from Ref. 11. The data for hafnium, molybdenum, niobium and tungsten are listed in Table III along with other pertinent properties. Additional data for other elements under consideration as possible seeding agents are also tabulated for reference.

A comparison was also made of the spectral absorption coefficients of tungsten at a temperature of 5000 K (based on the heavy-atom model) and the intensities of hafnium, molybdenum, niobium, and tungsten measured in an arc at 5100 K and reported in Ref. 11. These data are illustrated in Fig. 22 as a function of wave number.

It should be noted that the spectral absorption coefficients inferred by the line intensity data at wave numbers below approximately 24,000 cm^{-1} are much less than those predicted by the heavy-atom model. Therefore, it is extremely important to determine the true absorption in this spectral region because these spectral absorption coefficients are the primary contributors to the Rosseland mean opacity at low temperatures.

An additional consideration in selecting materials as possible seeding agents is the effect of the seed material on nuclear criticality. A summary of the nuclear cross-section data (Ref. 13) for possible seeding agents as a function of the average line spacing is presented in Fig. 23.

Ratio of Line Half-Width to Line Spacing in Gaseous Tungsten

The half-width of a collision broadened line is given by (Ref. 14):

$$\Gamma = \frac{1}{2C} \left(\frac{\beta_{op} a}{a_o} \right)^{2/5} \langle V_{op} \rangle^{3/5} N_p \qquad (11)$$

Where Γ is the line half-width in cm^{-1}. For tungsten-atomic hydrogen interactions the potential function coefficient β_{op} is of the order of 1.13 x 10^{-33} cm^6/sec; for tungsten-molecular hydrogen interactions, β_{op} is of the order of 1.40 x 10^{-33} cm^6/sec. The relative velocity for the tungsten-atomic hydrogen system is given by:

$$\langle V_{op} \rangle^{3/5} = 3.08 \times 10^2 \, T^{3/10} \qquad (12)$$

Similarly, the relative velocity for the tungsten-molecular hydrogen system is given by:

$$\langle V_{op} \rangle^{3/5} = 2.50 \times 10^2 \, T^{3/10} \qquad (13)$$

Equations (11) through (13) were used to compute the line half-width of a typical tungsten line broadened by both atomic and molecular hydrogen as a function of temperature and total hydrogen pressure. Because of low tungsten densities typically used for seed materials as compared to the hydrogen density ($\rho_\omega \simeq 0.03 \, \rho_{H_2}$), resonance or self-broadening was negligible. The half-widths based on Eqs. (11) and (12) are plotted in Fig. 24 as a function of temperature for hydrogen total pressures of 500 and 1000 atms. Line half-widths due to broadening by atomic and

molecular hydrogen as well as the total or combined half-widths are shown. The half-width resulting from molecular hydrogen broadening decreases with an increase in temperature due to the increasing dissociation of the molecular hydrogen as the temperature is raised. Similarly, the half-width resulting from atomic hydrogen broadening increases with an increase in temperature up to approximately 8000 K, but decreases with an increase in temperature above approximately 8000 K (due to subsequent ionization of the atomic hydrogen).

The results shown in Fig. 24 were used to compute the ratio of the line half-width to line spacing in tungsten as a function of temperature. These calculated results are illustrated in Fig. 25. Although the minimum average line spacing calculated for tungsten was the order of 13 cm^{-1} (see Fig. 21), a value for the average spacing of approximately 43 was used to allow for the fact that the wave number range treated in the model considerably exceeds that shown in Fig. 21

Spectral Absorption Parameter and Rosseland Mean Opacity Parameter of Gaseous Tungsten

Figure 26 illustrates the spectral absorption parameter (defined as the spectral absorption coefficient in cm^{-1} divided by the mass density) of gaseous tungsten for two temperatures (10,000 and 15,000 K) based on the heavy-atom model assuming completely overlapped lines. However, the spectral absorption parameters at low wave numbers are in doubt because of the results shown in Fig. 22. These results were used to compute the Rosseland mean opacity parameter (in cm^2/gm) for the completely overlapped line model as illustrated by the upper curve in Fig. 27. The lower curve in Fig. 27 is the Rosseland mean opacity parameter of gaseous tungsten allowing for a non-overlapping line structure as determined from the ratio of line half-width to line spacing (Fig. 25) and the results in Fig. 20. (Note that the use of the correction factor in the Rosseland mean absorption parameter implies that it is valid for the entire spectrum, although it is actually applicable only to the bound-bound spectral region.)

At a temperature of 5600 K (approximate boiling point of tungsten) the ratio of Rosseland mean opacity parameter assuming completely overlapped lines to the Rosseland mean opacity parameter corrected for non-overlapping line effects if of the order of 1.3. At a temperature of 15,000 K this ratio is of the order 2.6 and reflects the decrease in Γ (see Fig. 24) with an increase in temperature.

REFERENCES

1. Weinstein, H., and R. Ragsdale: The Coaxial Flow Reactor - A Gaseous Nuclear-Rocket Concept. ARS Reprint 1518-60, presented at the ARS 15th Annual Meeting, Washington, D. C., December 1960.

2. Ford, K. W.: Crude Estimate of Line Contribution to Uranium Opacity. UAC Research Laboratories Report UAR - 9044, May 1961.

3. Sziklas, E. A.: Method for Estimating the Opacity of a Heavy-Atom Gas. UAC Research Laboratories Report M-1688-1, September 1961.

4. Krascella, N. L.: Theoretical Investigation of the Spectral Opacities of Hydrogen and Nuclear Fuel. Air Force Systems Command Report RTD-TDR-63-1101 prepared by UAC Research Laboratories under Contract AF 04(611)-8189, November 1963.

5. Allen, C. W.: Astrophysical Quantities, Athlone Press, London, 1955.

6. Williamson, H. A., H. H. Michels, and S. B. Schneiderman: Theoretical Investigation of the Lowest Five Ionization Potentials of Uranium, Report D-910099-2 prepared by UAC Research Laboratories, September 1965.

7. Lanzo, C. D., and R. G. Ragsdale: Experimental Determination of Spectral and Total Transmissivities of Clouds of Small Particles. NASA Technical Note D-1405, September 1962.

8. Lanzo, C. D., and R. G. Ragsdale: Heat Transfer of a Seeded Flowing Gas From an Arc Enclosed by a Quartz Tube. NASA Technical Memorandum X-52005, June 1964.

9. Krascella, N. L.: Theoretical Investigation of the Absorption and Scattering Characteristics of Small Particles. Report C-910092-1 prepared by UAC Research Laboratories under Contract NASw-847, September 1964.

10. Marteney, P. J.: Experimental Investigation of the Opacity of Small Particles. Report C-910092-2 prepared by UAC Research Laboratories under Contract NASw-847, September 1964.

11. Meggers, W. F., C. H. Corliss, and B. F. Scribner: Table of Spectral-Line Intensities. National Bureau of Standards Monograph 32 - Part I, December 1961.

12. Moore, C. E.: Atomic Energy Levels. Circular of the National Bureau of Standards, Vol. I, June 1949; Vol. II, August 1952; Vol. III, May 1958.

13. Hughes, D. J., and J. A. Harvey: Neutron Cross Sections. U. S. Atomic Energy Commission, Brookhaven National Laboratory, McGraw-Hill Book Co., Inc., New York, 1955.

14. Ch'em, Shang-Yi, and Makoto Takeo: Broadening and Shift of Spectral Lines Due to the Presence of Foreign Gases. Reviews of Modern Physics, Vol. 29, No. 1, January 1957.

LIST OF SYMBOLS

a_i — Energy level spacing in heavy-atom model, ev

a — Constant $= 3\pi/8$

a_R — Rosseland mean opacity, cm^{-1} (see Eq. (8))

a_ω — Spectral absorption coefficient without stimulated emission, cm^{-1}

a_ω^* — Spectral absorption coefficient with stimulated emission, cm^{-1}

$\bar{a}$ — Mean opacity $= (1/S) \sum_{ALL\ LINES} a_\omega d\omega$, cm^{-1}

$\bar{\bar{a}}$ — Mean opacity $= \left[(1/S) \int \dfrac{d\omega}{\sum_{ALL\ LINES} a_\omega} \right]$, cm^{-1}

b_R — Rosseland mean opacity parameter, cm^2/gm

b_ω^* — Spectral absorption parameter with stimulated emission, cm^2/gm

B_ω — Black-body function (see Eq. (9))

c — Velocity of light $= 2.998 \times 10^{10}$ cm/sec

E — Photon energy, ev

$(\overset{\circ}{E})_i$ — Cut-off energy for ionization species i used in oscillator strength estrapolation, ev

$(E_n)_i$ — Energy of the nth level in ionization species i of the heavy-atom model, ev

f_i — Total oscillator strength of the ith ionization species

$F^\circ, F^+, F^{++}, F^{+++}$ — Denote various fuel ionization species

G — Partition function parameter used in heavy-atom model (See Eqs. (2) and (3))

h — Planck's constant $= 6.6237 \times 10^{-27}$ erg-sec

I_i Ionization potential of the ith ionization species, ev

k Boltzmann constant $= 1.380 \times 10^{-16}$ erg/deg K

K A constant (see Eq. (2))

n Quantum number defining an energy level in the heavy-atom model

N_e Electron particle density, cm^{-3}

N_i Particle density of ith ionization species, cm^{-3}

N_p Particle density of a perturber species, cm^{-3}

Q_i Partition function of the ith ionization species

S Line spacing, cm^{-1}

T Temperature, K

V_{ap} Relative velocity of perturber and absorber, cm/sec

$(X_n)_i$ Ionization potential from the nth energy level of species i, ev

α_o "Weisskopf phase," a constant $\simeq 1.0$

β_{ap} Van der Waal's potential function coefficient, cm^6/sec

Γ Spectral line half-width, cm^{-1}

ρ Mass density, gm/cm^3

ω Wave number, cm^{-1}

ω_o Wave number at line center, cm^{-1}

Subscripts

a Absorber species

e^- Electrons

i Ionization species

p   Perturber species

ω Spectral quantity

TABLE I

PARAMETRIC VARIATIONS USED IN HEAVY-ATOM MODEL STUDIES OF NUCLEAR FUEL OPACITY

*   Case 1 represents "standard case" and is based on parameter values formerly used for heavy-atom opacity calculations in Ref. 4

**   See Fig. 5 for values of G

***   Ionization potentials reported in Ref. 6

Case	Ionization Potential, ev				Energy Level Spacing, ev				Total Oscillator Strength				Partition Function Parameter
	$I\ F^{0}$	$I\ F^{+}$	$I\ F^{++}$	$I\ F^{+++}$	$a\ F^{0}$	$a\ F^{+}$	$a\ F^{++}$	$a\ F^{+++}$	$n\ F^{0}$	$n\ F^{+}$	$n\ F^{++}$	$n\ F^{+++}$	G
1 *	6.0	10.0	18.0	28.0	0.40	0.40	0.40	0.40	2.0	2.0	2.0	2.0	1.0
2	6.0	10.0	18.0	28.0	0.20	0.20	0.20	0.20	2.0	2.0	2.0	2.0	1.0
3	6.0	10.0	18.0	28.0	0.05	0.05	0.05	0.05	2.0	2.0	2.0	2.0	1.0
4	6.0	10.0	18.0	28.0	0.40	0.40	0.40	0.40	1.0	1.0	1.0	1.0	1.0
5	6.0	10.0	18.0	28.0	0.20	0.20	0.20	0.20	1.0	1.0	1.0	1.0	1.0
6	6.0	10.0	18.0	28.0	0.05	0.05	0.05	0.05	1.0	1.0	1.0	1.0	1.0
7	6.0	10.0	18.0	28.0	0.40	0.40	0.40	0.40	2.0	2.0	2.0	2.0	5.0
8	6.0	10.0	18.0	28.0	0.1	0.2	0.3	0.4	2.0	2.0	2.0	2.0	1.0
9	6.0	10.0	18.0	28.0	0.40	0.40	0.40	0.40	0.50	1.0	1.5	2.0	1.0
10	6.0	10.0	18.0	28.0	0.40	0.40	0.40	0.40	2.0	2.0	2.0	2.0	Variable**
11	6.0	12.0	24.0	48.0	0.40	0.40	0.40	0.40	2.0	2.0	2.0	2.0	1.0
12	6.1	17.1	38.8	65.6***	0.40	0.40	0.40	0.40	2.0	2.0	2.0	2.0	1.0

TABLE II

COMPARISON OF ROSSELAND MEAN OPACITIES FOR DIFFERENT VALUES OF INPUT PARAMETERS IN HEAVY-ATOM MODEL FOR A PRESSURE OF 1000 ATM

NOTES: Tabulated values for Case 1 are Rosseland mean opacities, $\sigma_R - cm^{-1}$.
Tabulated values for Cases 2 - 12 are ratios, $\sigma_R/(\sigma_R)_{CASE\ 1}$.
See Table I for parameters employed in each case.

TEMPERATURE, T - DEG K

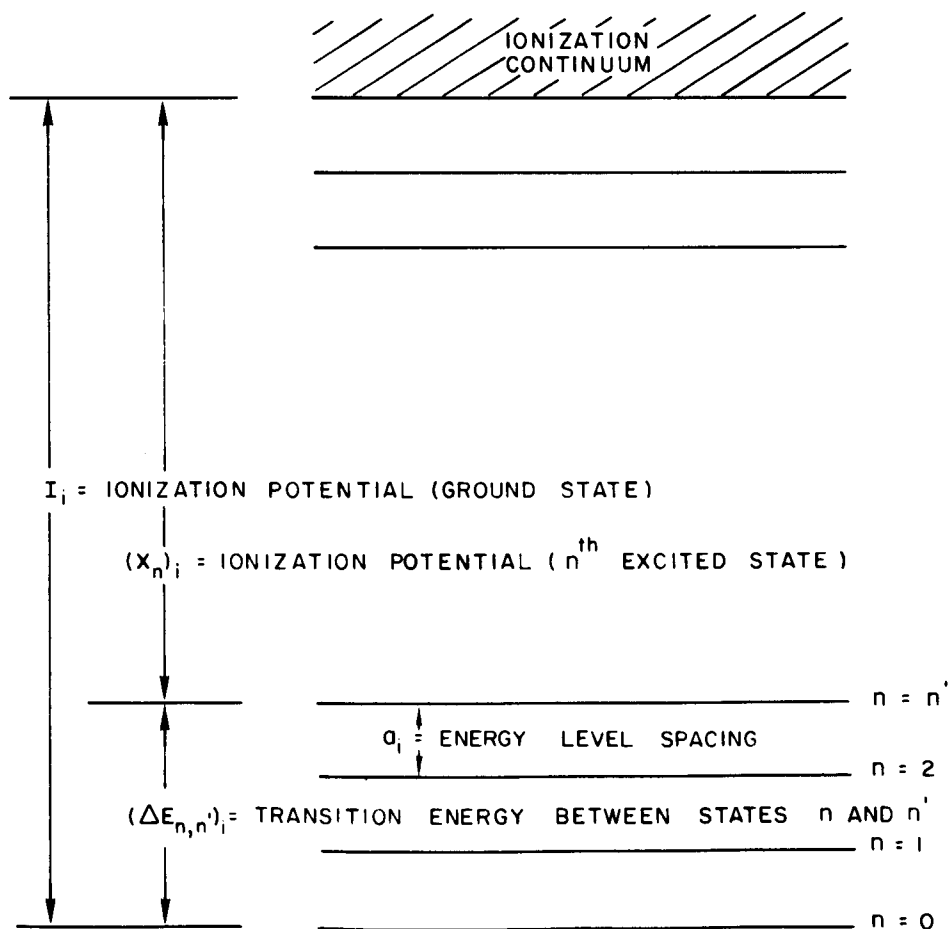| CASE	10,000	12,500	15,000	17,500	20,000	25,000	30,000	35,000	40,000	45,000	50,000	55,000	60,000	65,000	70,000	75,000	80,000	85,000	90,000	95,000	100,000
1	3044	1260	684.5	460.1	350.5	202.4	109.8	67.83	45.78	31.76	22.34	15.84	11.28	8.089	5.865	4.319	3.239	2.475	1.928	1.529	1.233
2	0.973	0.981	0.988	0.991	0.990	1.001	0.998	1.010	1.018	1.019	1.017	1.013	1.008	1.004	1.001	0.999	0.997	0.995	0.994	0.993	0.992
3					0.980		0.996	0.996	1.031		1.028		1.014				0.994				0.987
4	0.958	0.974	0.975	0.966	0.958	0.956	0.959	0.959	0.961	0.979	0.986	0.991	0.994	0.996	0.997	0.998	0.999	0.999	0.999	1.000	1.000
5					0.949		0.957		0.987		1.003		1.003								0.992
6					0.940		0.956		1.000		1.014		1.008				0.993				0.986
7					1.428		1.337		1.139		1.037		1.012				1.003				1.001
8					0.991		0.996		0.998		1.000		1.000				1.000				1.000
9					0.978		0.994		0.999		1.000		1.000				1.000				1.000
10	1.000		1.003		1.002		1.002		1.008				1.002				1.001				1.000
11	1.085	1.194	1.271	1.273	1.251	1.373	1.494	1.555	1.852	2.335	2.761	3.040	3.203	3.299	3.359	3.398	3.427	3.448	3.465	3.478	3.488
12	1.311		2.305		1.966	1.664	1.664	2.163	2.774	2.720	2.810	3.199	3.877	4.673	5.404		6.405		6.888		7.089

TABLE III

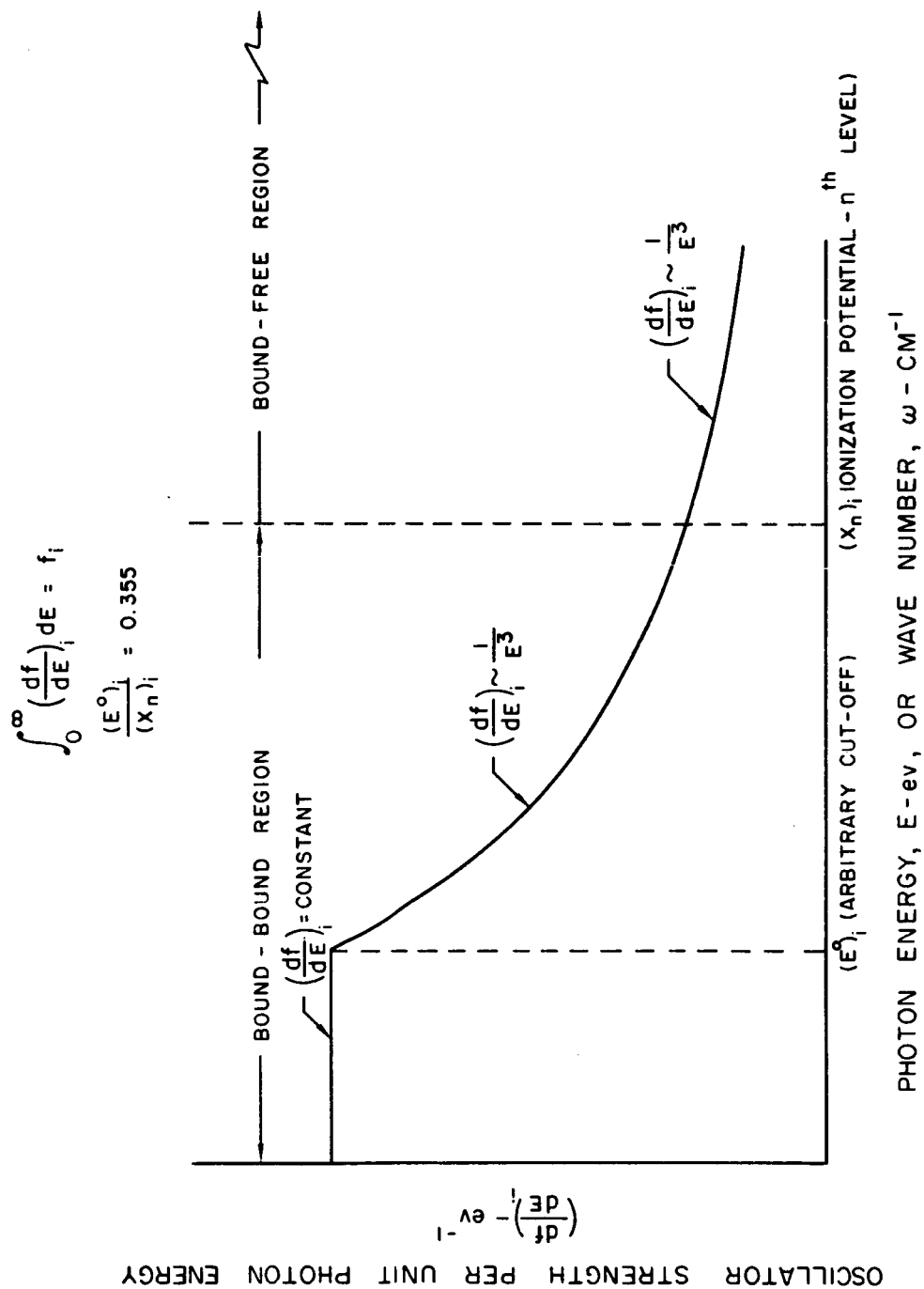AVERAGE SPACING BETWEEN KNOWN LINES IN CERTAIN HEAVY-ATOM GASES

NOTES: Number of lines and corresponding wave number range from Ref. 12, which gives total number of classified lines independent of line strengths. Nuclear cross sections from Ref. 13.

Element	Symbol	Atomic Weight	Density gm/cm³	Density lb/ft³	Melting Point, deg R	Boiling Point, deg R	Nuclear Cross-Section, barns	Number of Lines	Wave Number Range cm⁻¹		Average Line Spacing, cm⁻¹
Cobalt	Co	58.94	8.90	555	3182	4550	37	2725	8408	55127	17.1
Hafnium	Hf	178.60	13.3	830	4050	10728	105	2000	8304	52138	21.9
Iridium	Ir	193.10	22.40	1398	4909	8010	430	4000	11637	49975	9.58
Iron	Fe	55.85	7.86	491	3216	5481	2.53	4860	8352	53908	9.39
Molybdenum	Mo	95.95	10.20	636	5202	9180	2.5	7500	8439	50000	6.88
Niobium	Nb	92.91	8.55	534	4986	9207	1.1	3313	9157	46253	11.2
Palladium	Pd	106.70	11.97	747	3281	6093	8.0	390	10830	58005	12.1
Platinum	Pt	195.23	21.45	1338	3677	7164	8.1	440	9295	15042	13.1
Rhenium	Re	186.31	20.53	1281	6215	10647	84	4200	8482	58824	12.0
Rhodium	Rh	102.91	12.4	774	4030	7092	150	950	11608	50302	40.7
Silicon	Si	28.06	2.42	151	3029	5202	0.13	400	8150	64856	160
Tantalum	Ta	180.88	16.60	1036	5886	10017	21.3	2300	8237	51203	18.2
Tungsten	W	183.92	19.30	1204	6570	10161	19.2	3700	9544	56054	12.8
Vanadium	V	50.95	5.96	372	3942	5891	5.1	2186	8396	48031	18.1
Zirconium	Zr	91.22	6.4	400	3825	8276	0.18	1600	10779	47870	23.2

ENERGY LEVEL DIAGRAM FOR THE HEAVY – ATOM MODEL

(i – REFERS TO ith IONIZATION SPECIES)

n = QUANTUM NUMBER

IONIZATION CONTINUUM

I_i = IONIZATION POTENTIAL (GROUND STATE)

$(X_n)_i$ = IONIZATION POTENTIAL (nth EXCITED STATE)

n = n'

a_i = ENERGY LEVEL SPACING

n = 2

$(\Delta E_{n,n'})_i$ = TRANSITION ENERGY BETWEEN STATES n AND n'

n = 1

n = 0

ASSUMED DISTRIBUTION OF OSCILLATOR STRENGTH PER UNIT PHOTON ENERGY AS A FUNCTION OF PHOTON ENERGY FOR THE HEAVY-ATOM MODEL

$$\int_0^\infty \left(\frac{df}{dE}\right)_i dE = f_i$$

$$\frac{(E^0)_i}{(x_n)_i} = 0.355$$

BOUND-FREE REGION

BOUND-BOUND REGION

$$\left(\frac{df}{dE}\right)_i \sim \frac{1}{E^3}$$

$$\left(\frac{df}{dE}\right)_i \sim \frac{1}{E^3}$$

$$\left(\frac{df}{dE}\right)_i = \text{CONSTANT}$$

$(E^0)_i$ (ARBITRARY CUT-OFF)

$(x_n)_i$ IONIZATION POTENTIAL-n^{th} LEVEL)

PHOTON ENERGY, E-ev, OR WAVE NUMBER, ω-CM^{-1}

OSCILLATOR STRENGTH PER UNIT PHOTON ENERGY $\left(\frac{df}{dE}\right)_i$-ev^{-1}

EFFECT OF TEMPERATURE ON THE CALCULATED PARTITION FUNCTIONS DERIVED FROM ENERGY LEVEL DISTRIBUTION EMPLOYED IN HEAVY-ATOM MODEL

RESULTS SHOWN WERE CALCULATED FOR IONIZATION POTENTIALS
AND ENERGY LEVEL SPACING FOR CASE I, AND WERE USED TO
COMPUTE PARTITION FUNCTION RATIOS SHOWN IN FIG. 4

$$Q_i = \sum_n \exp\left\{-(E_n)_i / kT\right\}$$

$(E_n)_i$ – ENERGY OF THE nth LEVEL IN IONIZATION
SPECIES i OF THE HEAVY-ATOM MODEL
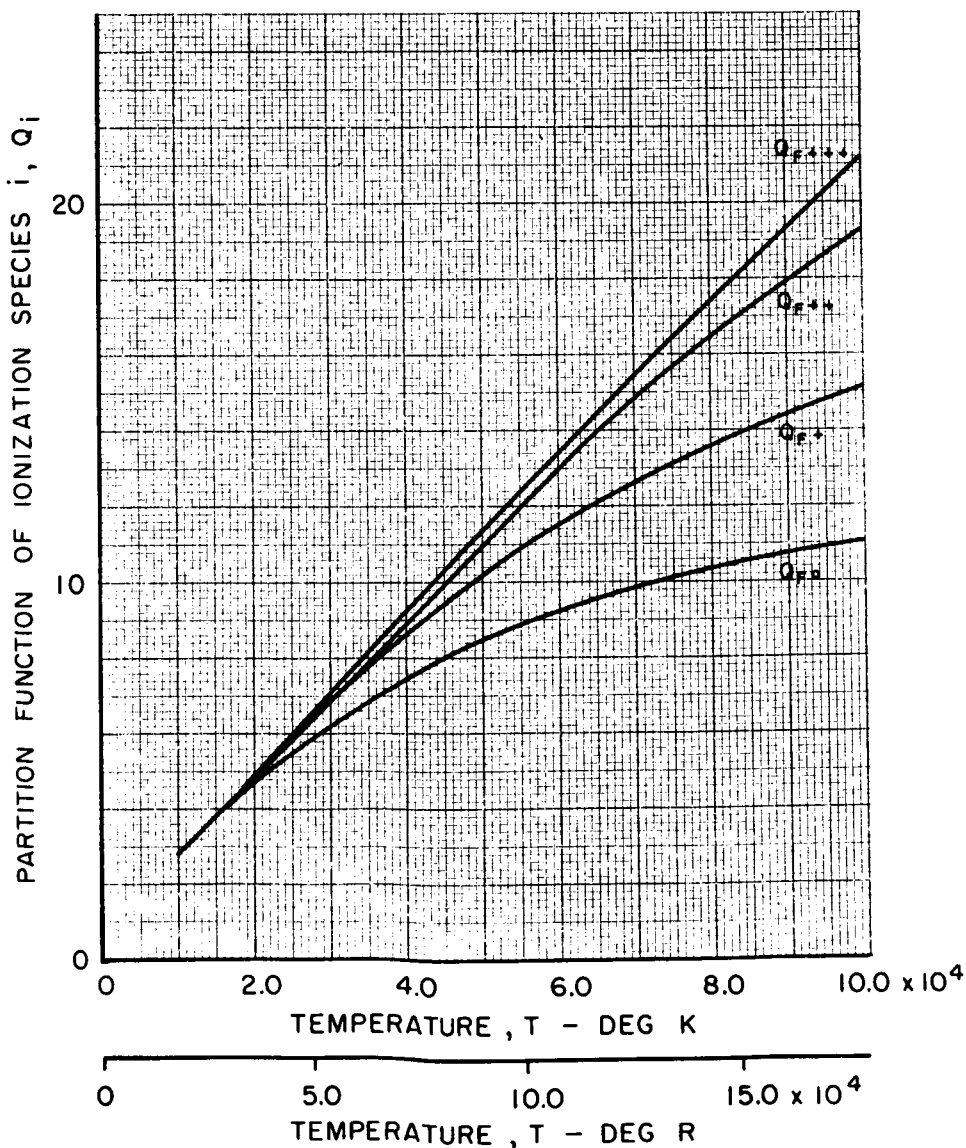
EFFECT OF TEMPERATURE ON THE CALCULATED HEAVY-ATOM MODEL PARTITION FUNCTION RATIOS DERIVED FROM ENERGY LEVEL DISTRIBUTION EMPLOYED IN HEAVY-ATOM MODEL

Q_i AND Q_{i+1} FROM FIG. 3

AVERAGE VALUE OF Q_{i+1}/Q_i AT EACH TEMPERATURE

EQUAL TO PARTITION FUNCTION PARAMETER G, FOR

CASE 10 SHOWN IN FIG. 5

FIG. 5
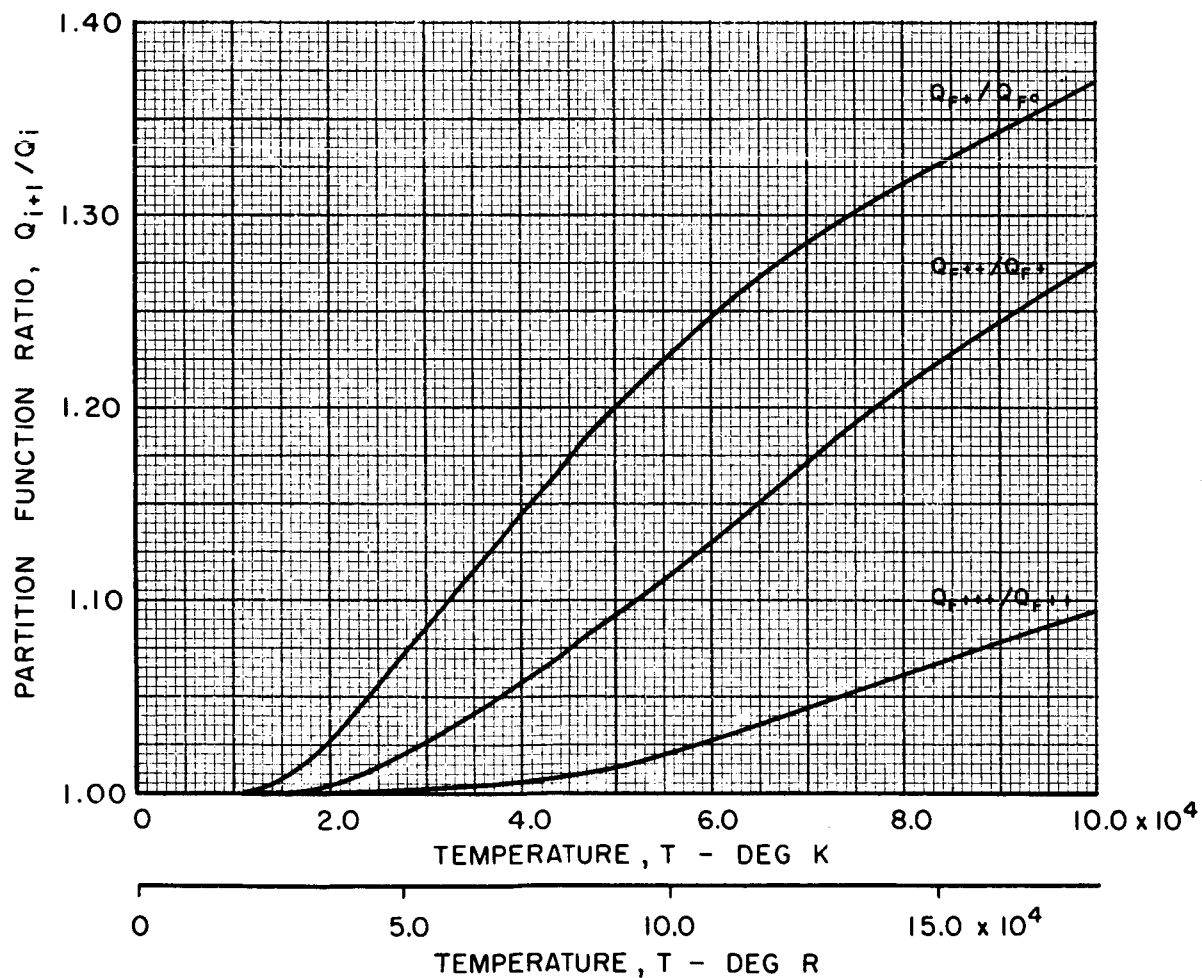
EFFECT OF TEMPERATURE ON PARTITION FUNCTION PARAMETERS EMPLOYED IN CALCULATION OF NUCLEAR FUEL COMPOSITION

SEE FIGS. 3 AND 4 AND TABLE I FOR CASE 10,

$$G = \frac{1}{3}\left[\frac{Q_{F^+}}{Q_{F^0}} + \frac{Q_{F^{++}}}{Q_{F^+}} + \frac{Q_{F^{+++}}}{Q_{F^{++}}}\right]$$
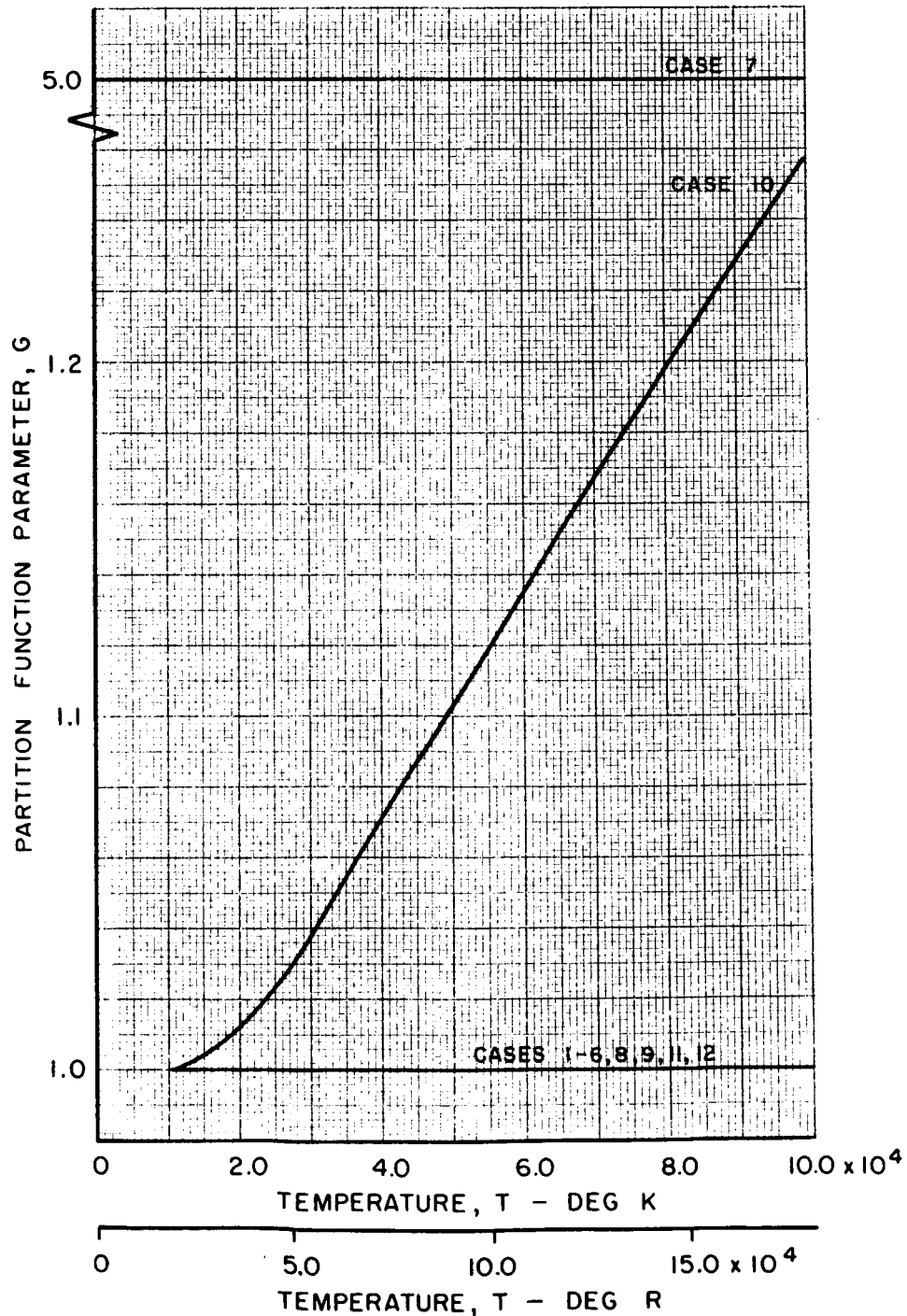
COMPARISON OF THE EFFECT OF TEMPERATURE ON
THE COMPOSITION OF NUCLEAR FUEL FOR DIFFERENT
VALUES OF THE PARTITION FUNCTION PARAMETER USED IN
THE HEAVY-ATOM MODEL AT 1000 ATM TOTAL PRESSURE

SEE FIG. 5 AND TABLE I
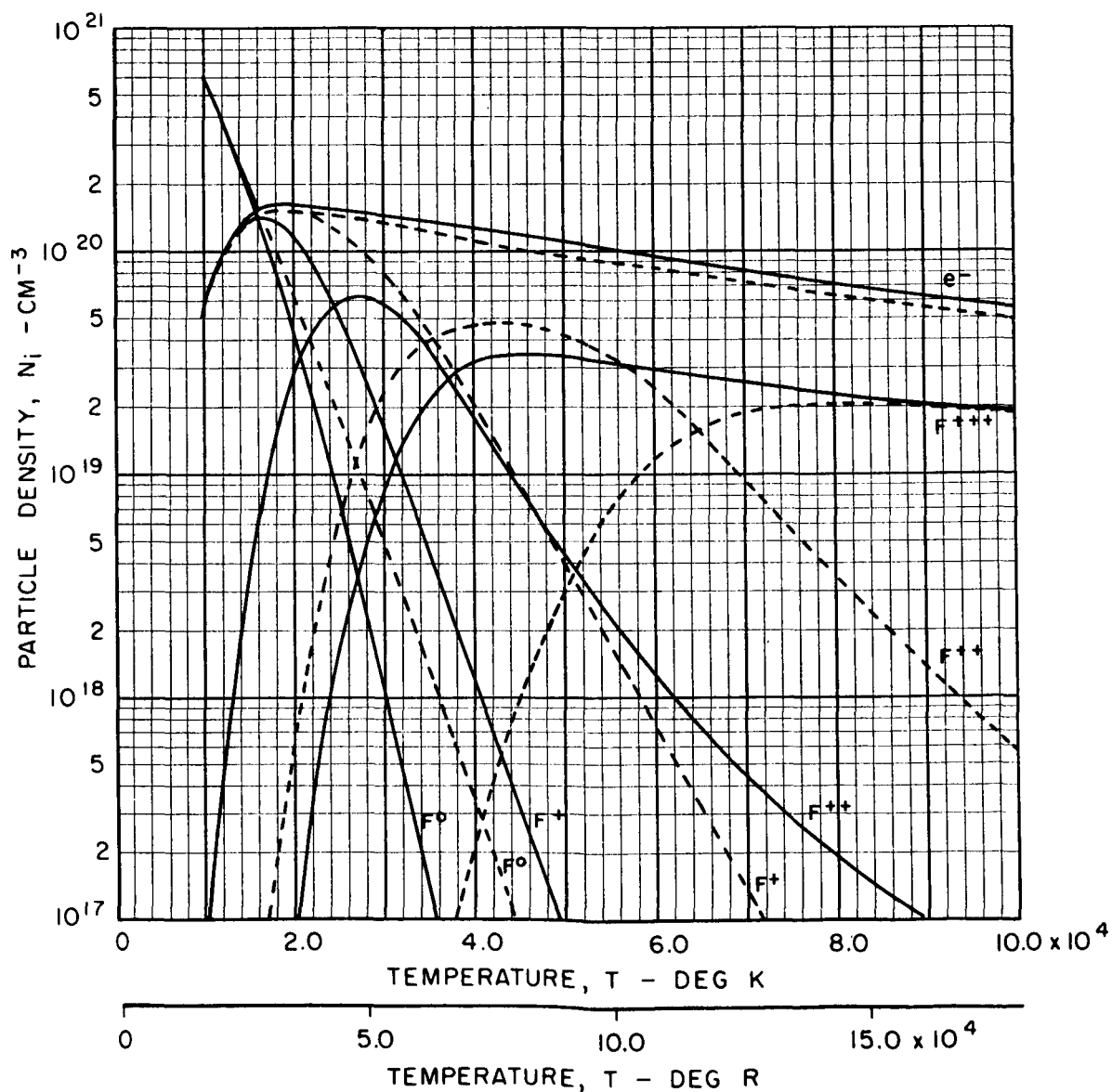
————— CASE 1

— —·—— CASE 7

— — — — CASE 10

COMPARISON OF THE EFFECT OF TEMPERATURE ON COMPOSITION OF NUCLEAR FUEL FOR DIFFERENT IONIZATION POTENTIALS USED IN THE HEAVY-ATOM MODEL AT 100 ATM TOTAL PRESSURE

CURVE	CASE NO. (SEE TABLE I)	IONIZATION POTENTIALS							
		I_{F^0}		I_{F^+}		$I_{F^{++}}$		$I_{F^{+++}}$	
		ev	CM^{-1}	ev	CM^{-1}	ev	CM^{-1}	ev	CM^{-1}
———	1	6	48402	10	80670	18	145206	28	225876
– – –	12	6.1	49210	17.1	137946	38.8	313000	65.6	529195

COMPARISON OF THE EFFECT OF TEMPERATURE
ON COMPOSITION OF NUCLEAR FUEL FOR DIFFERENT
IONIZATION POTENTIALS USED IN THE HEAVY-ATOM MODEL
AT 500 ATM TOTAL PRESSURE

CURVE	CASE NO. (SEE TABLE I)	IONIZATION POTENTIALS							
		I_{F^o}		I_{F^+}		$I_{F^{++}}$		$I_{F^{+++}}$	
		ev	CM^{-1}	ev	CM^{-1}	ev	CM^{-1}	ev	CM^{-1}
———	1	6	48402	10	80670	18	145206	28	225876
– – –	12	6.1	49210	17.1	137946	38.8	313000	65.6	529195

COMPARISON OF THE EFFECT OF TEMPERATURE ON COMPOSITION OF NUCLEAR FUEL FOR DIFFERENT IONIZATION POTENTIALS USED IN THE HEAVY-ATOM MODEL AT 1000 ATM TOTAL PRESSURE

CURVE	CASE NO. (SEE TABLE I)	IONIZATION POTENTIALS							
		I_{F^0}		I_{F^+}		$I_{F^{++}}$		$I_{F^{+++}}$	
		ev	CM⁻¹	ev	CM⁻¹	ev	CM⁻¹	ev	CM⁻¹
———	1	6	48402	10	80670	18	145206	28	225876
- - - -	12	6.1	49210	17.1	137946	38.8	313000	65.6	529195

COMPARISON OF EFFECT OF WAVE NUMBER ON SPECTRAL
ABSORPTION COEFFICIENT OF NUCLEAR FUEL FOR VARIOUS
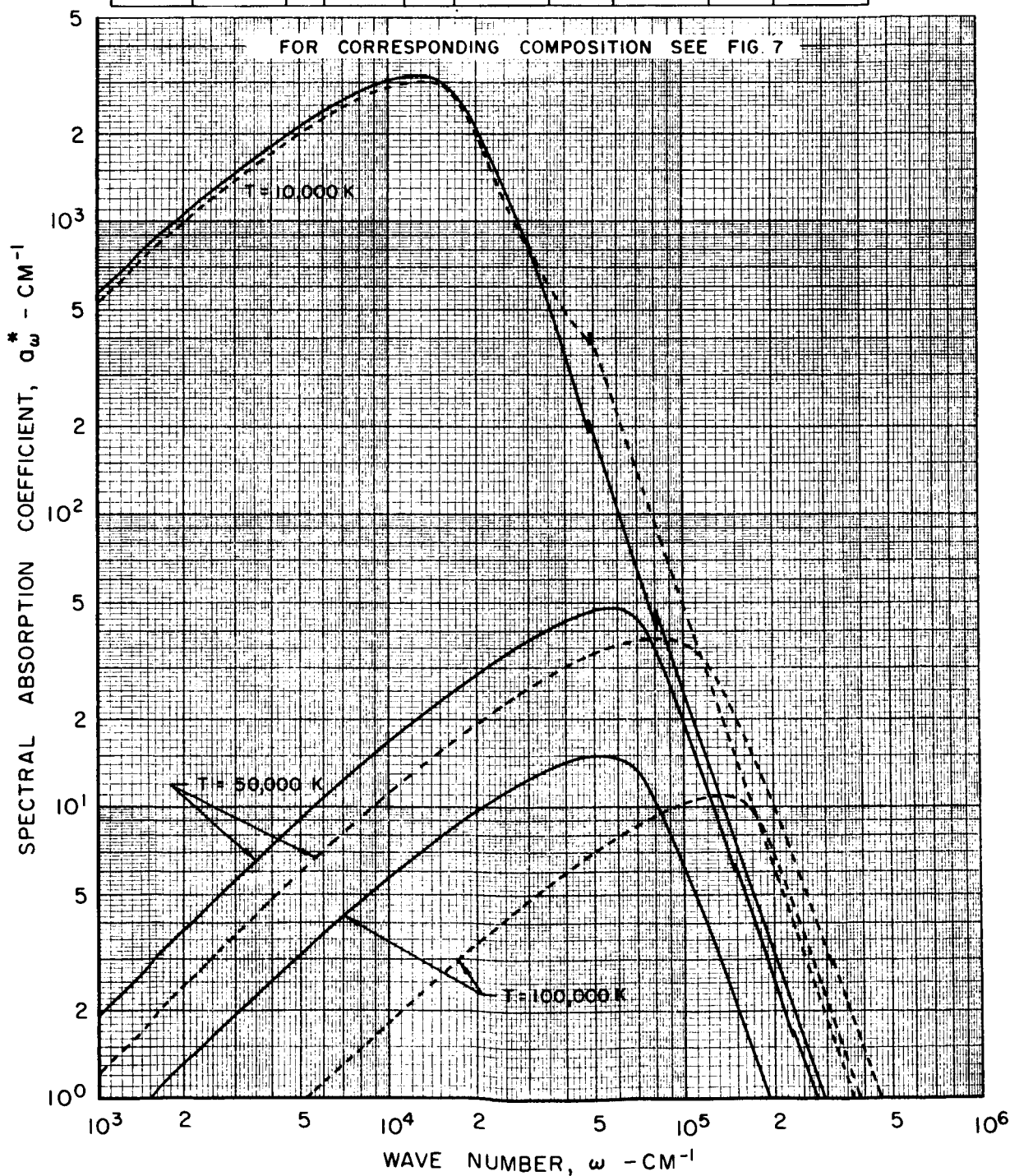PARAMETRIC CHANGES IN THE HEAVY - ATOM
MODEL AT 20,000 DEG K

TOTAL PRESSURE = 1000 ATM

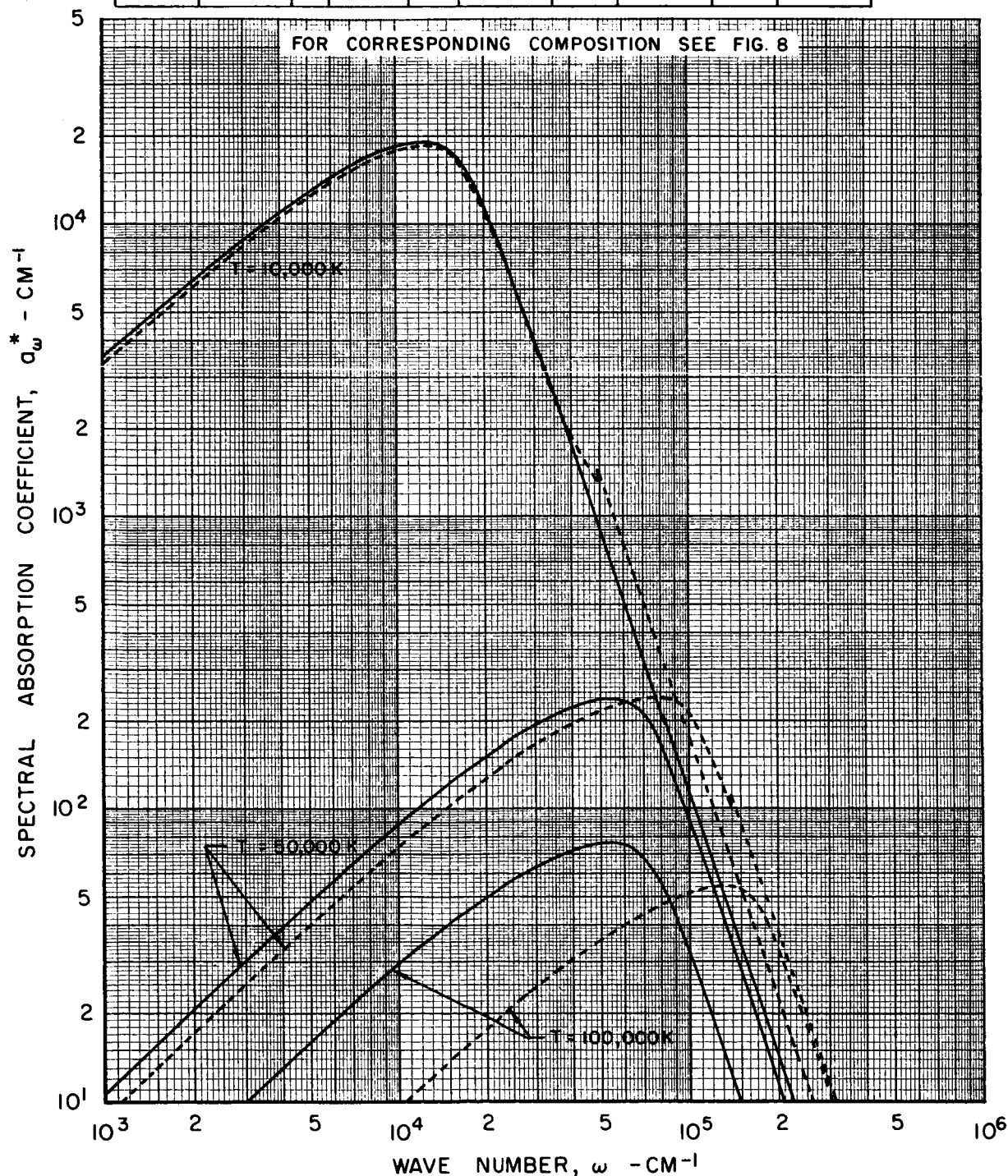NUMERALS ON CURVES REFER TO CASE NUMBERS
LISTED IN TABLE I

FIG. II

COMPARISON OF EFFECT OF WAVE NUMBER ON SPECTRAL ABSORPTION COEFFICIENT OF NUCLEAR FUEL FOR VARIOUS PARAMETRIC CHANGES IN THE HEAVY – ATOM MODEL AT 60,000 DEG K

TOTAL PRESSURE = 1000 ATM

NUMERALS ON CURVES REFER TO CASE NUMBERS
LISTED IN TABLE I
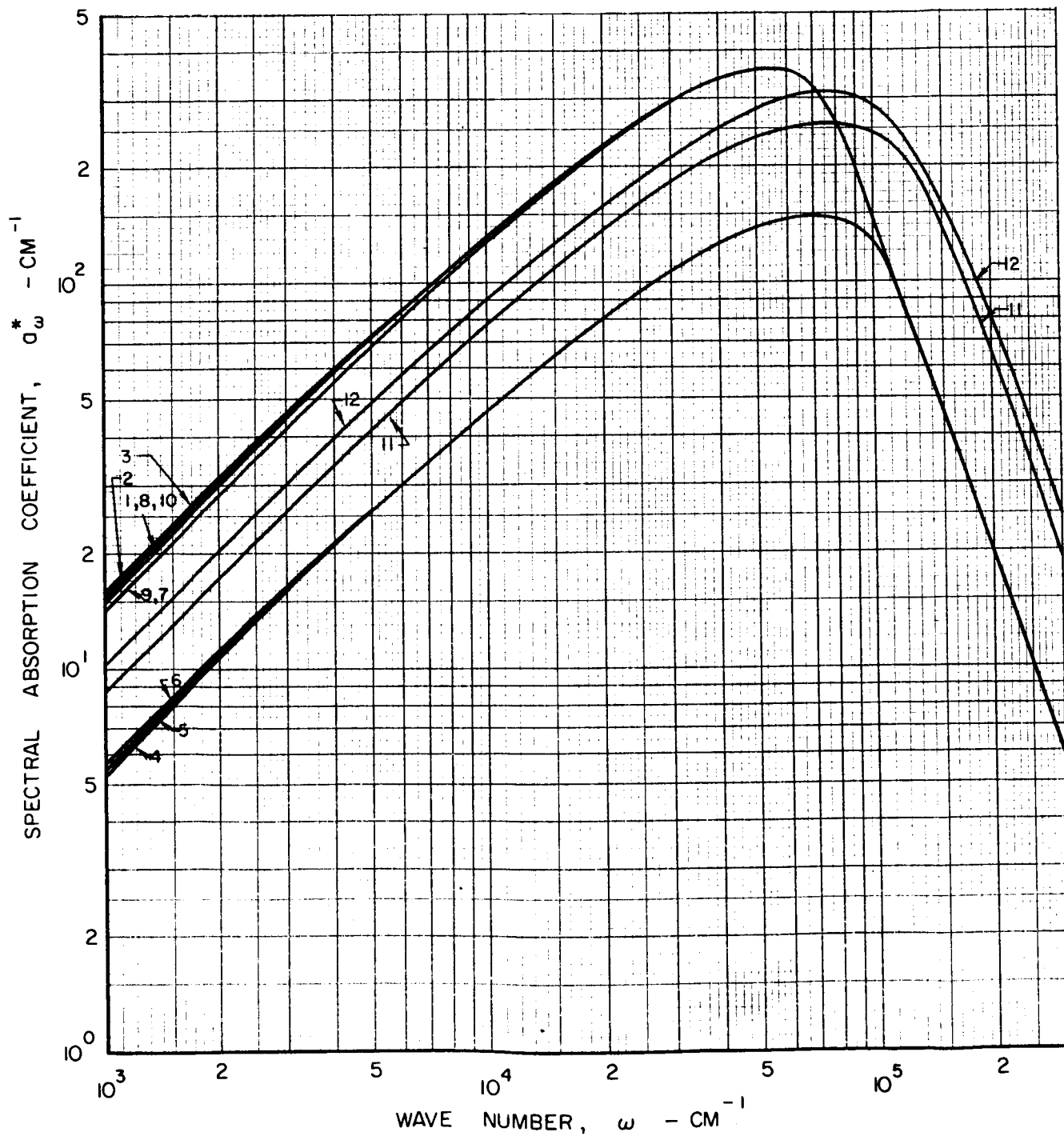
COMPARISON OF EFFECT OF WAVE NUMBER ON SPECTRAL ABSORPTION COEFFICIENT OF NUCLEAR FUEL FOR VARIOUS PARAMETRIC CHANGES IN THE HEAVY-ATOM MODEL AT 100,000 DEG K

TOTAL PRESSURE = 1000 ATM

NUMERALS ON CURVES REFER TO CASE NUMBERS
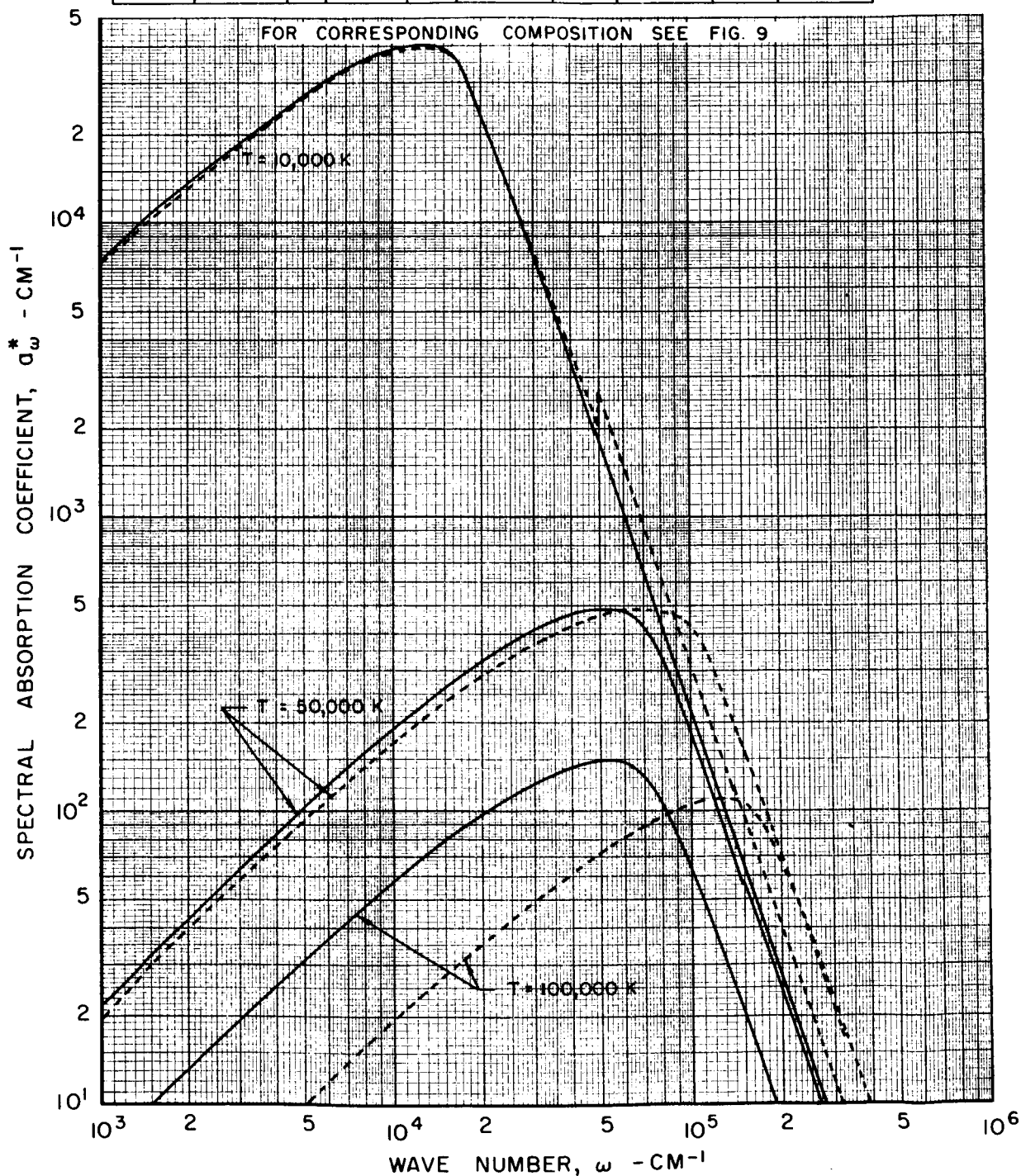LISTED IN TABLE I

COMPARISON OF THE EFFECT OF WAVE NUMBER ON THE
SPECTRAL ABSORPTION COEFFICIENT OF NUCLEAR FUEL FOR
DIFFERENT IONIZATION POTENTIALS USED IN THE HEAVY-ATOM
MODEL AT 100 ATM TOTAL PRESSURE

CURVE	CASE NO. (SEE TABLE I)	IONIZATION POTENTIALS							
		I_{F^0}		I_{F^+}		$I_{F^{++}}$		$I_{F^{+++}}$	
		ev	CM⁻¹	ev	CM⁻¹	ev	CM⁻¹	ev	CM⁻¹
———	1	6	48402	10	80670	18	145206	28	225876
- - - -	12	6.1	49210	17.1	137946	38.8	313000	65.6	529195

FOR CORRESPONDING COMPOSITION SEE FIG. 7

FIG. 14

COMPARISON OF THE EFFECT OF WAVE NUMBER ON THE SPECTRAL ABSORPTION COEFFICIENT OF NUCLEAR FUEL FOR DIFFERENT IONIZATION POTENTIALS USED IN THE HEAVY-ATOM MODEL AT 500 ATM TOTAL PRESSURE
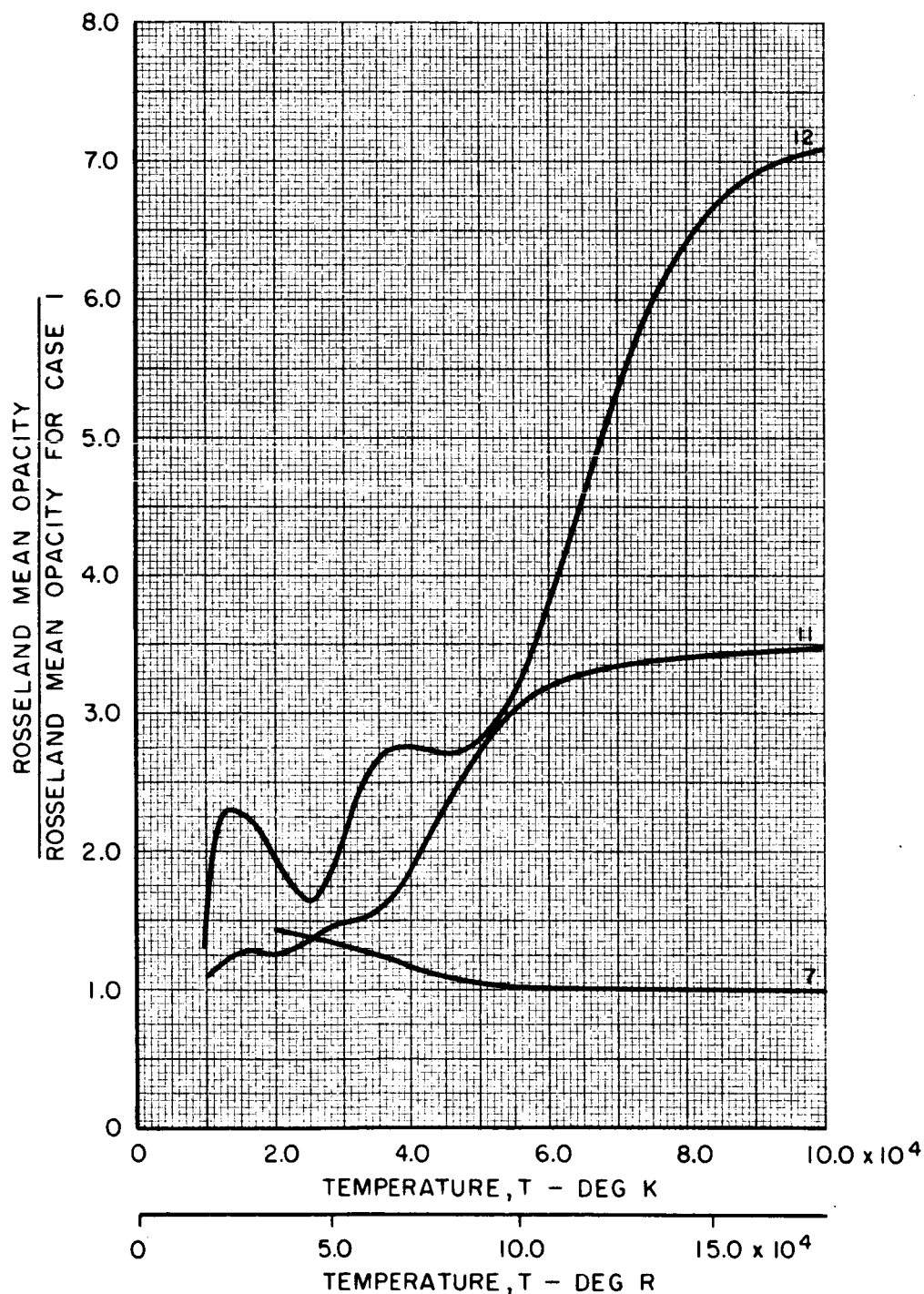
CURVE	CASE NO. (SEE TABLE I)	IONIZATION POTENTIALS							
		I_{F^o}		I_{F^+}		$I_{F^{++}}$		$I_{F^{+++}}$	
		ev	CM^{-1}	ev	CM^{-1}	ev	CM^{-1}	ev	CM^{-1}
———	1	6	48402	10	80670	18	145206	28	225876
— — —	12	6.1	49210	17.1	137946	38.8	313000	65.6	529195

FOR CORRESPONDING COMPOSITION SEE FIG. 8

SPECTRAL ABSORPTION COEFFICIENT, a_ω^* - CM^{-1}

WAVE NUMBER, ω -CM^{-1}

COMPARISON OF THE EFFECT OF WAVE NUMBER ON THE SPECTRAL ABSORPTION COEFFICIENT OF NUCLEAR FUEL FOR DIFFERENT IONIZATION POTENTIALS USED IN THE HEAVY-ATOM MODEL AT 1000 ATM TOTAL PRESSURE

| CURVE | CASE NO. (SEE TABLE I) | IONIZATION POTENTIALS | | | | | | | |
| | | I_{F^0} | | I_{F^+} | | $I_{F^{++}}$ | | $I_{F^{+++}}$ | |
		ev	CM⁻¹	ev	CM⁻¹	ev	CM⁻¹	ev	CM⁻¹
———	1	6	48402	10	80670	18	145206	28	225876
– – –	12	6.1	49210	17.1	137946	38.8	313000	65.6	529195

EFFECT OF TEMPERATURE ON THE RATIO OF ROSSELAND
MEAN OPACITY FOR CASES 7, 11 AND 12 TO THE ROSSELAND
MEAN OPACITY FOR CASE 1

TOTAL PRESSURE = 1000 ATM

NUMERALS ON CURVES REFER TO CASE NUMBERS LISTED IN TABLE 1

COMPARISON OF THE EFFECT OF TEMPERATURE ON THE ROSSELAND MEAN OPACITY OF NUCLEAR FUEL FOR DIFFERENT IONIZATION POTENTIALS USED IN THE HEAVY-ATOM MODEL

CURVE	CASE NO. (SEE TABLE I)	IONIZATION POTENTIALS							
		I_{F^o}		I_{F^+}		$I_{F^{++}}$		$I_{F^{+++}}$	
		ev	CM^{-1}	ev	CM^{-1}	ev	CM^{-1}	ev	CM^{-1}
———	1	6	48402	10	80670	18	145206	28	225876
– – – –	12	6.1	49210	17.1	137946	38.8	313000	65.6	529195

FOR CORRESPONDING SPECTRAL ABSORPTION COEFFICIENTS SEE FIGS. 13 TO 15

FIG. 18

SPECTRAL ABSORPTION COEFFICIENT DISTRIBUTIONS
ASSUMED IN PARAMETRIC STUDY OF HEAVY – ATOM MODEL

BOUND-BOUND REGION $(0 < \omega < 50,000 \ CM^{-1})$
$\int a_\omega \, d\omega$ EQUAL FOR ALL DISTRIBUTIONS

BOUND-FREE REGION $(50,000 \ CM^{-1} < \omega < 700,000 \ CM^{-1})$
a_ω EQUAL FOR ALL DISTRIBUTIONS AND VARIES AS ω^{-3}
VALUE OF a_ω AT $700,000 \ CM^{-1}$ IS $2.92 \times 10^{-4} \ CM^{-1}$

FIG. 19
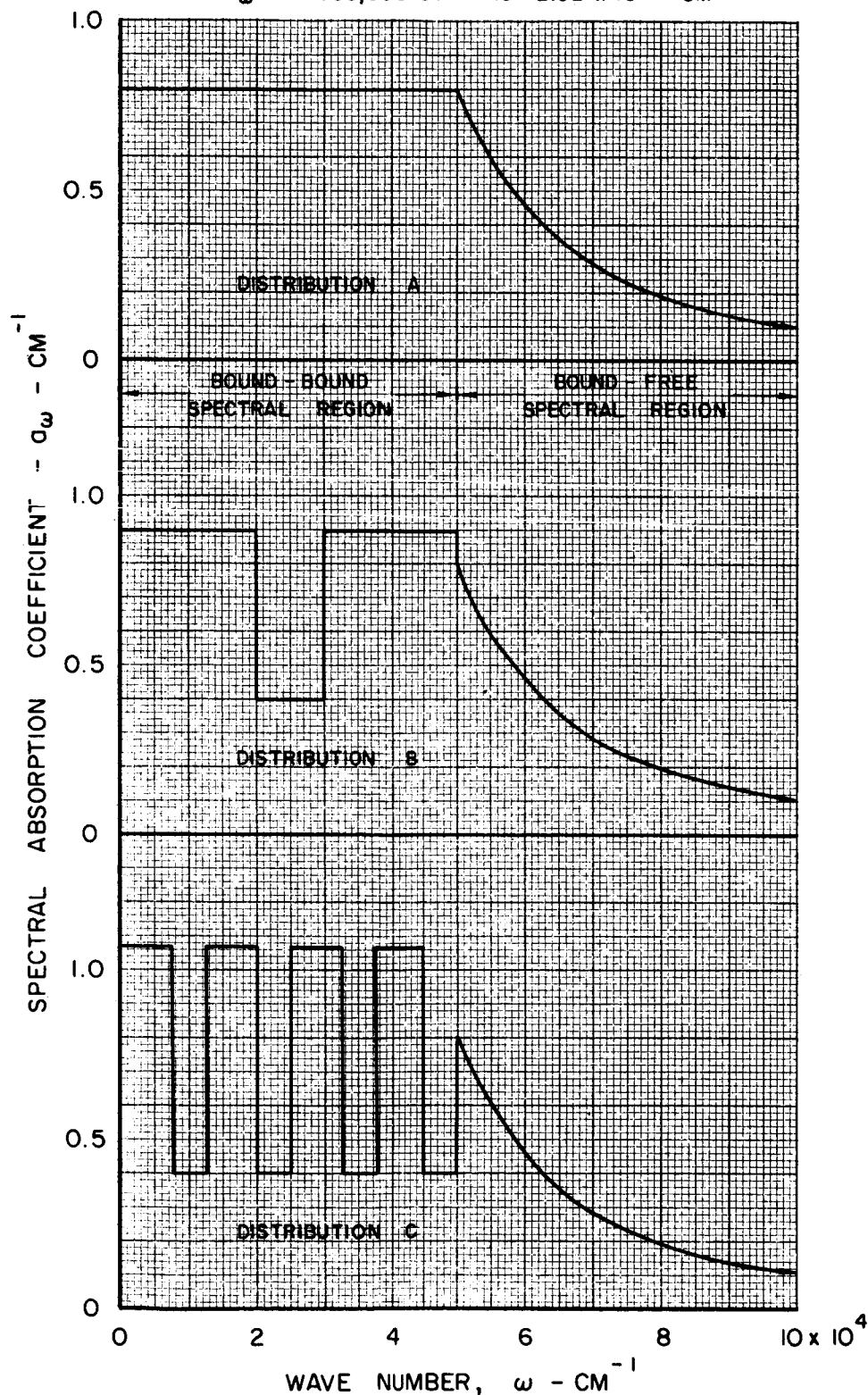
COMPARISON OF THE EFFECT OF TEMPERATURE ON THE ROSSELAND MEAN OPACITY FOR DIFFERENT ASSUMED DISTRIBUTIONS OF SPECTRAL ABSORPTION COEFFICIENTS IN THE BOUND – BOUND SPECTRAL REGION

ASSUMED VARIATION OF a_ω WITH ω FOR EACH DISTRIBUTION ILLUSTRATED IN FIG. 18

$$a_R = \frac{\int_{100}^{700,000} \frac{dB\omega}{dT} d\omega}{\int_{100}^{700,000} \frac{1}{a_\omega^*} \frac{dB\omega}{dT} d\omega}$$

$$a_\omega^* = a_\omega \left(1 - e^{-hc\omega/kT} \right)$$

DISTRIBUTION

A
B
C

ROSSELAND MEAN OPACITY, a_R – ARBITRARY UNITS

TEMPERATURE, T – DEG K

TEMPERATURE, T – DEG R
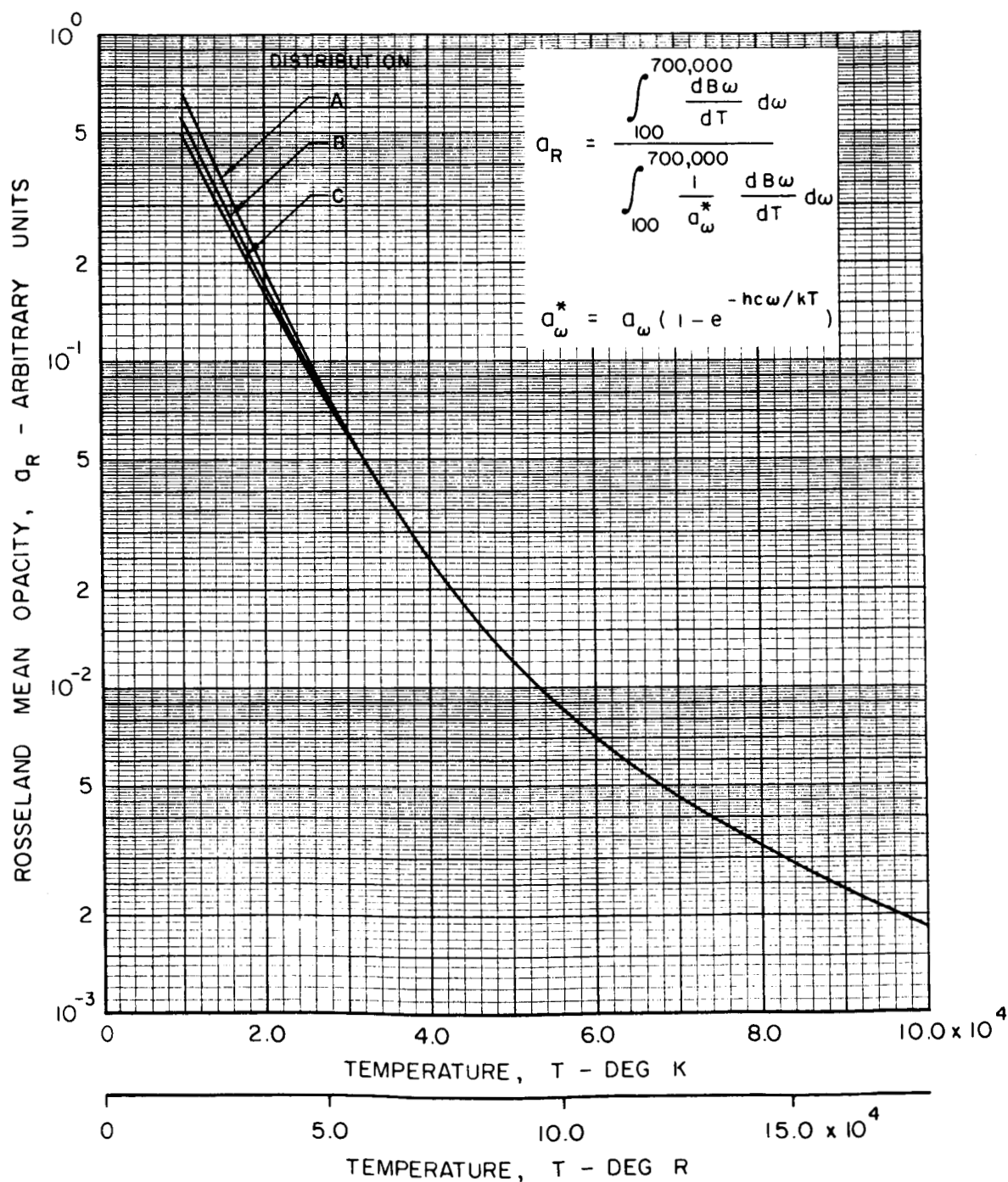
EFFECT OF RATIO OF LINE HALF-WIDTH TO LINE SPACING ON THE OPACITY CHARACTERISTICS OF A NON-OVERLAPPING LINE SPECTRUM
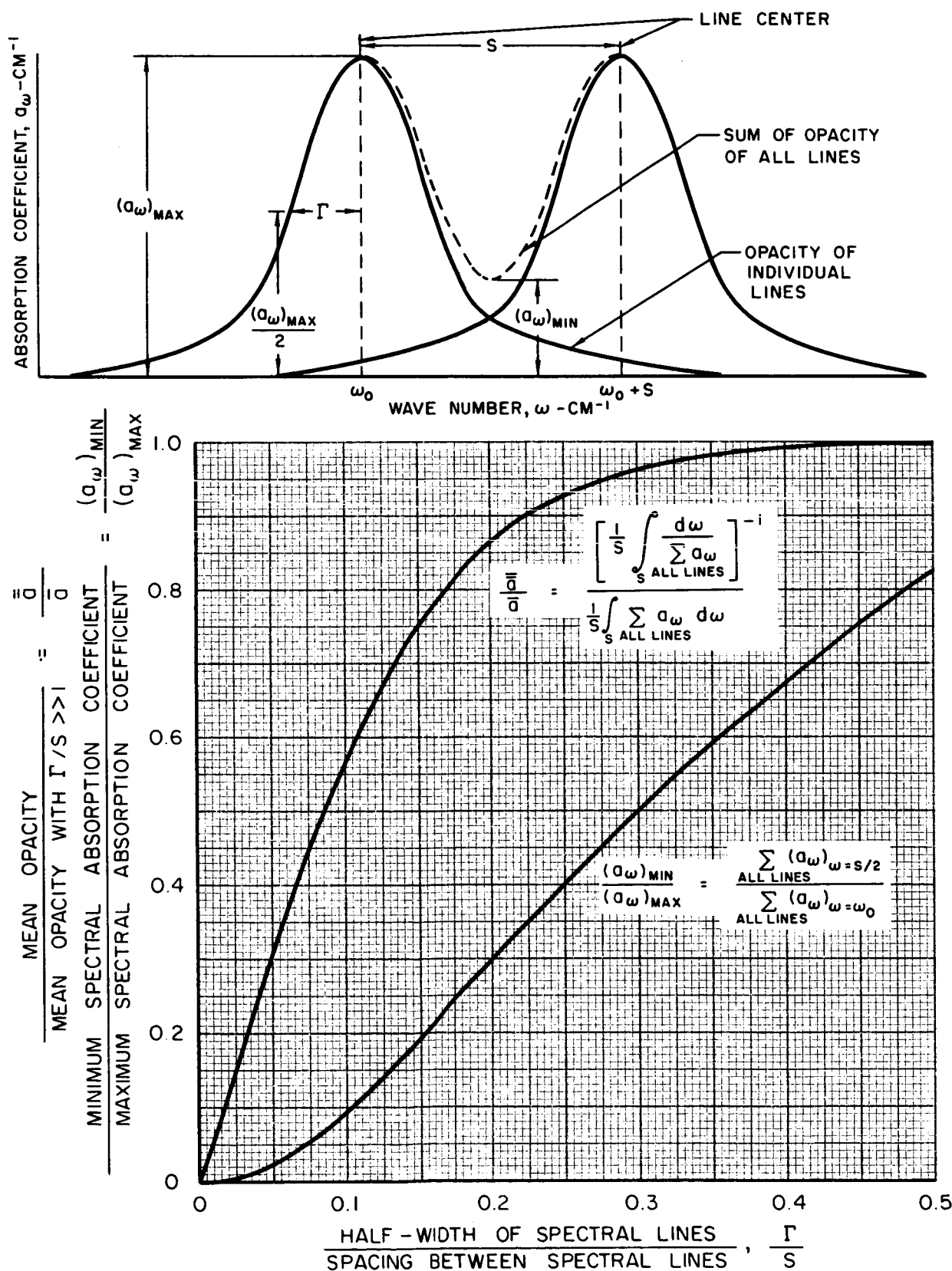
LOCAL AVERAGE LINE SPACING IN 1000 CM⁻¹ INTERVALS FROM KNOWN LINE STRUCTURE OF TUNGSTEN, NIOBIUM, MOLYBDENUM AND HAFNIUM

FIG. 22
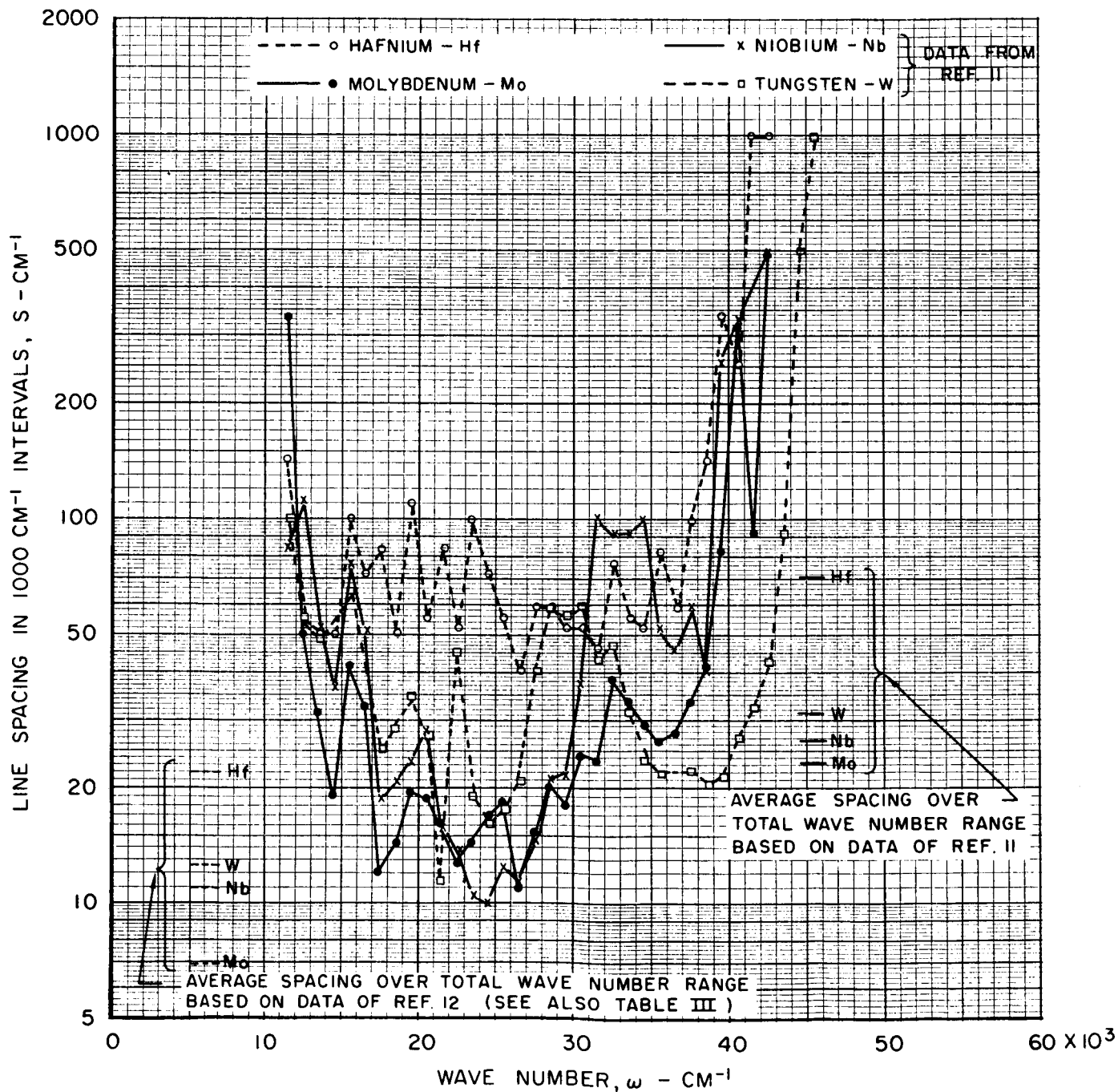
COMPARISON OF DISTRIBUTION OF SPECTRAL INTENSITY FROM ARC MEASUREMENTS
AND SPECTRAL ABSORPTION COEFFICIENT FROM HEAVY – ATOM MODEL

----- ○ HAFNIUM - Hf   ─── x NIOBIUM - Nb

● MOLYBDENUM - Mo   ------ □ TUNGSTEN - W

(DETERMINED FROM SUMMATION OF ALL KNOWN INTENSITIES OF
SPECTRAL LINES IN WAVE NUMBER INTERVALS OF 1000 CM⁻¹
INTENSITIES MEASURED IN ARC AT TEMPERATURE OF
APPROXIMATELY 5100 K (SEE REF. 11))

THEORETICAL SPECTRAL ABSORPTION COEFFICIENT OF TUNGSTEN
GAS FROM HEAVY - ATOM MODEL AT TEMPERATURE OF 5000 K
(SEE REF. 4)
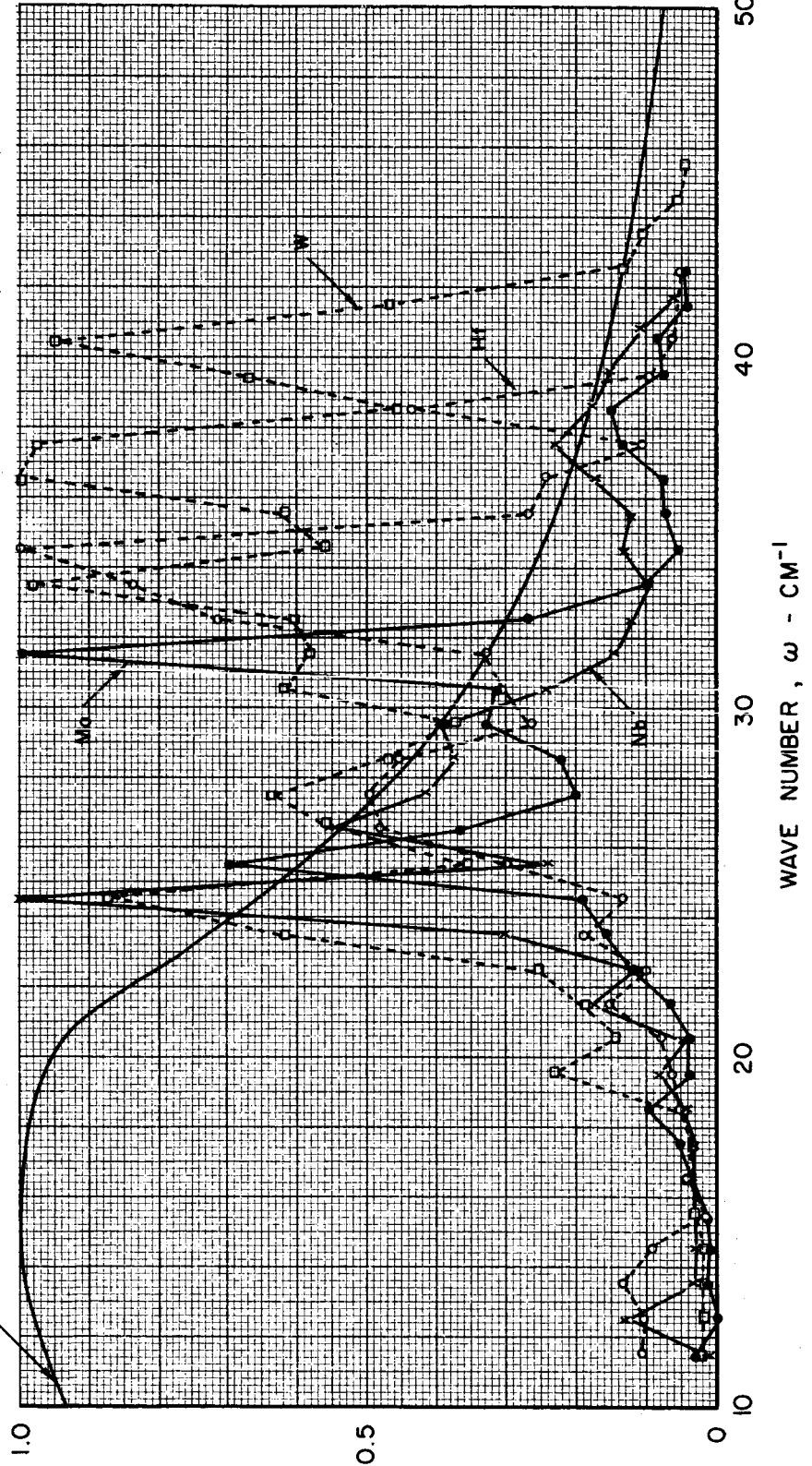
LINE SPACING AND NEUTRON ABSORPTION CROSS-SECTION FOR SEVERAL HEAVY-ATOM GASES

NUMBER OF LINES AND CORRESPONDING WAVE NUMBER RANGE FROM REF. 12,

WHICH GIVES TOTAL NUMBER OF CLASSIFIED LINES INDEPENDENT OF LINE STRENGTHS

NEUTRON CROSS SECTIONS FROM REF. 13.

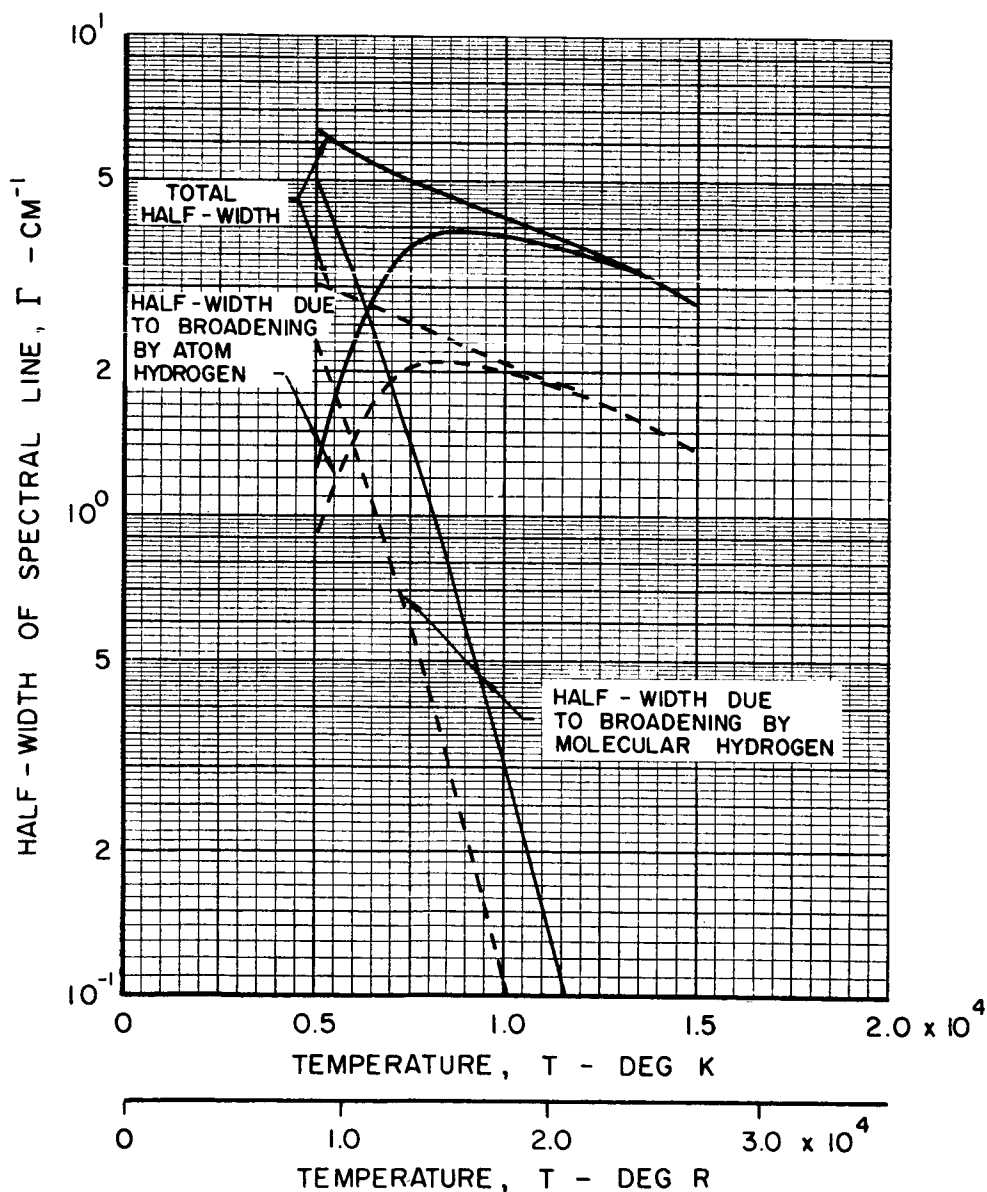NUMBER FOLLOWING CHEMICAL SYMBOL OF EACH ELEMENT DENOTES BOILING POINT
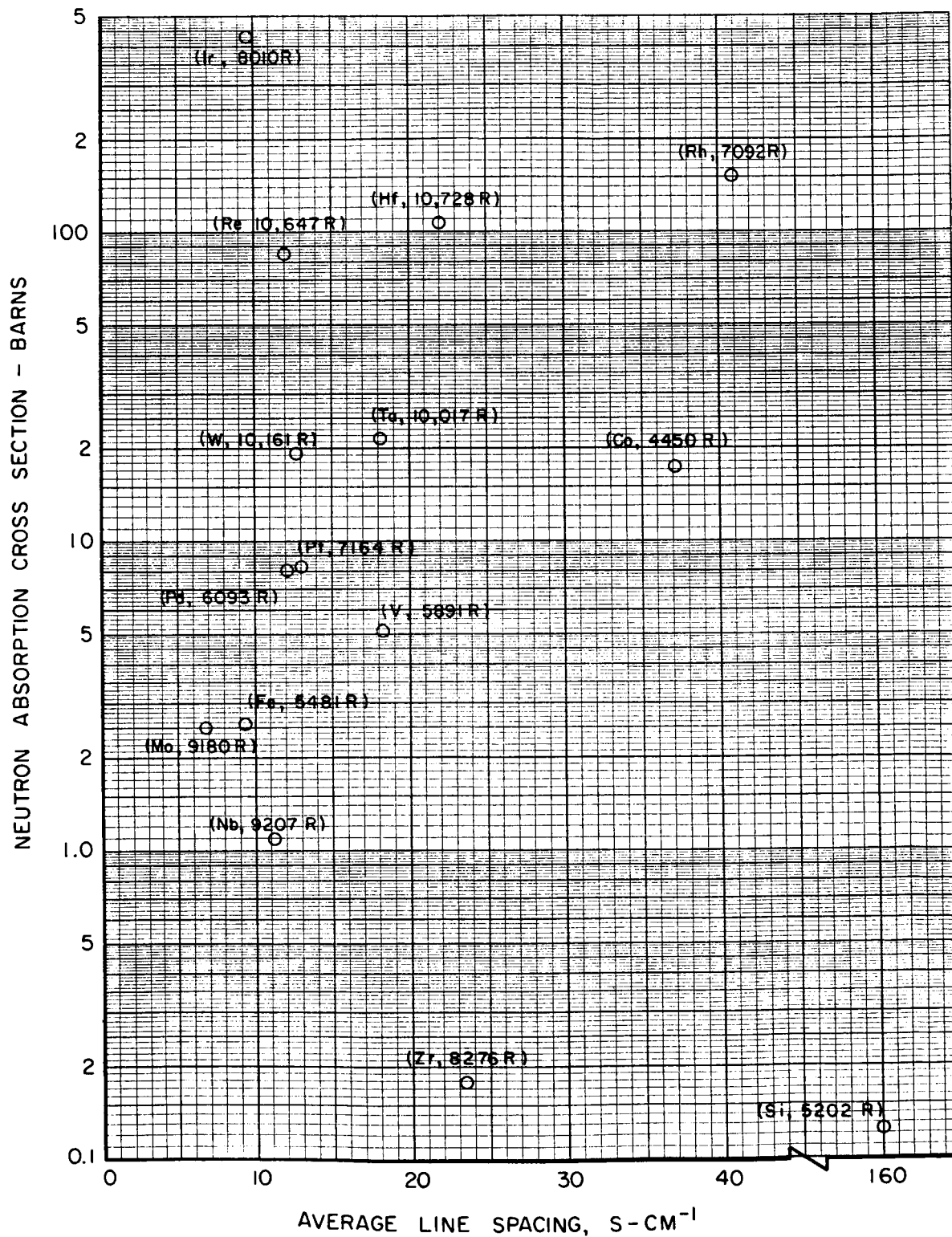
EFFECT OF TEMPERATURE ON THEORETICAL HALF-WIDTH OF SPECTRAL LINES IN TUNGSTEN GAS DUE TO BROADENING BY HYDROGEN

——————— HYDROGEN PRESSURE = 1000 ATM

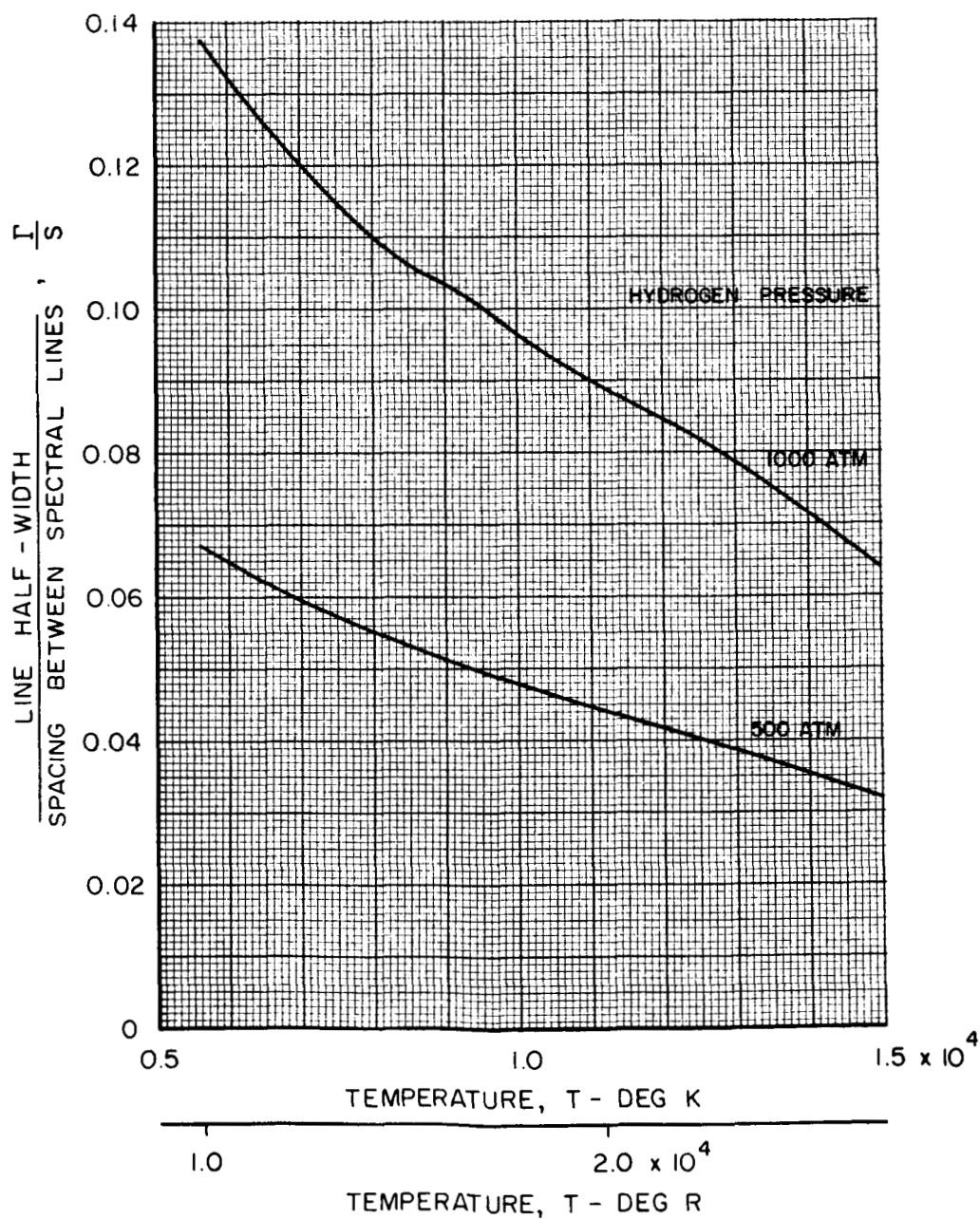— — — — — HYDROGEN PRESSURE = 500 ATM

(Γ INDEPENDENT OF TUNGSTEN DENSITY FOR SMALL TUNGSTEN DENSITIES)

FIG. 25

EFFECT OF TEMPERATURE ON THE RATIO OF HALF-WIDTH TO THE SPACING BETWEEN SPECTRAL LINES IN TUNGSTEN GAS
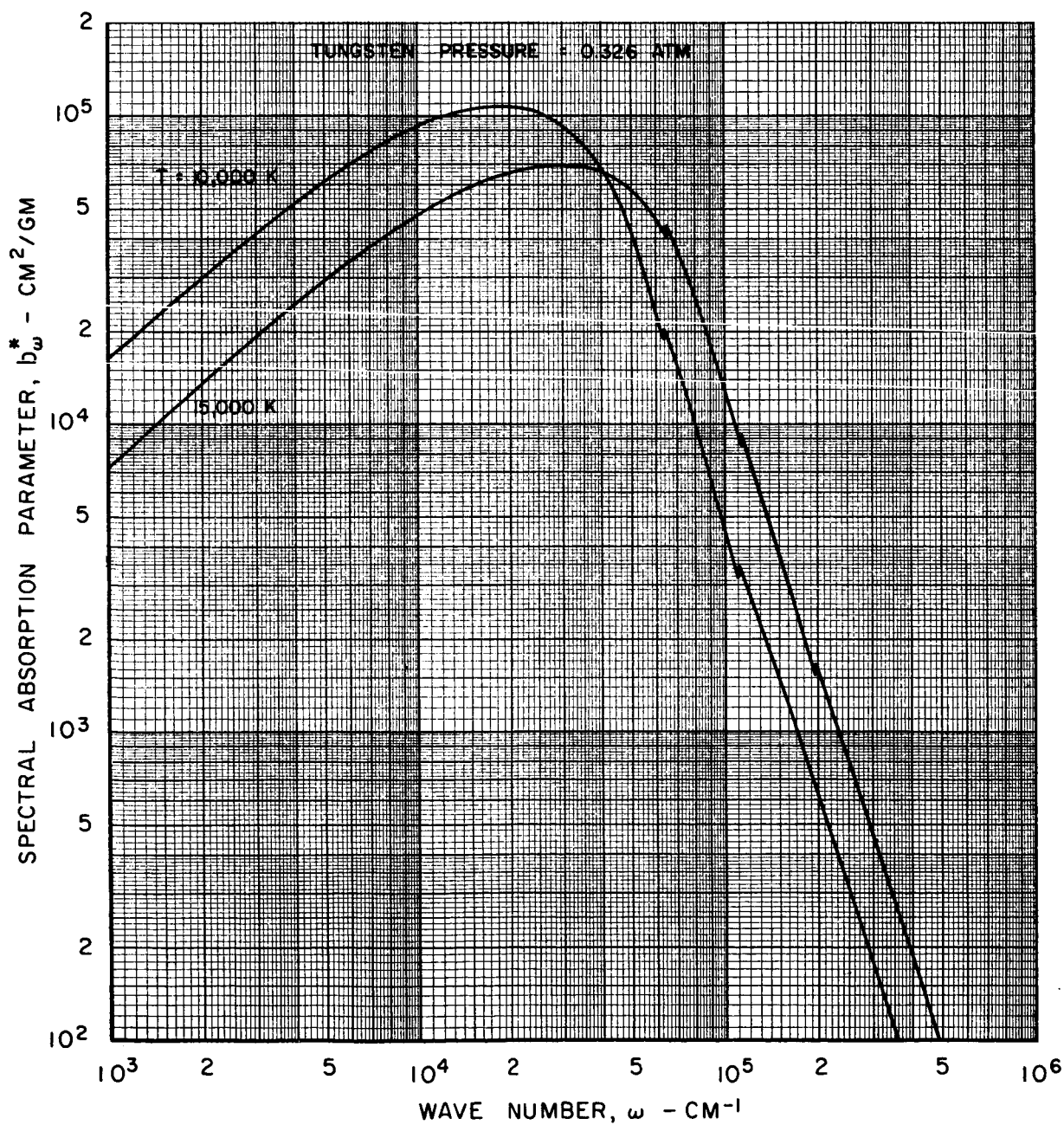
MEAN SPACING, S = 43.4 CM^{-1}

Γ FROM FIG. 24

EFFECT OF WAVE NUMBER ON THE SPECTRAL ABSORPTION PARAMETER OF TUNGSTEN GAS

COMPLETELY OVERLAPPED LINES
ASSUMED IN HEAVY-ATOM MODEL

EFFECT OF TEMPERATURE ON THE ROSSELAND MEAN OPACITY PARAMETER OF TUNGSTEN GAS

TUNGSTEN GAS PRESSURE = 0.326 ATM